Article

The Effect of the El Nino Southern Oscillation on Precipitation Extremes in the Hindu Kush Mountains Range

Muhammad Umer Masood [1], Saif Haider [2,3], Muhammad Rashid [2], Muhammad Usama Khan Lodhi [2], Chaitanya B. Pande [3,4,5,*], Fahad Alshehri [3], Kaywan Othman Ahmed [6], Miklas Scholz [7,8,9,10,11,12,*] and Saad Sh. Sammen [13]

1   Geological Engineering Department, Montana Technological University, Butte, MT 59701, USA
2   Centre of Excellence in Water Resources Engineering, University of Engineering and Technology, Lahore 54890, Pakistan; m.rashid.6122@gmail.com (M.R.)
3   Abdullah Alrushaid Chair for Earth Science Remote Sensing Research, Geology and Geophysics Department, King Saud University, Riyadh 11451, Saudi Arabia
4   Institute of Energy Infrastructure, Universiti Tenaga Nasional, Kajang 43000, Malaysia
5   New Era and Development in Civil Engineering Research Group, Scientific Research Center, Al-Ayen University, Nasiriyah 64001, Thi-Qar, Iraq
6   Department of Civil Engineering, Faculty of Engineering, Tishk International University-Sulaimani, Sulaymaniyah 46001, Kurdistan Region, Iraq; kaywan.osman@tiu.edu.iq
7   Innovation Management Department, aconium GmbH (previously atene KOM), Invalidenstraße 91, 10115 Berlin, Germany
8   Department of Civil Engineering Science, School of Civil Engineering and the Built Environment, Kingsway Campus, University of Johannesburg, Aukland Park, P.O. Box 524, Johannesburg 2006, South Africa
9   Directorate of Engineering, School of Science, Engineering and Environment, The University of Salford, Newton Building, Greater Manchester M5 4WT, UK
10 Department of Town Planning, Engineering Networks and Systems, South Ural State University, 76, Lenin Prospekt, 454080 Chelyabinsk, Russia
11 Kunststoff-Technik Adams, Specialist Company According to Water Law, Schulstraße 7, 26931 Elsfleth, Germany
12 Nexus by Sweden, Skepparbacken 5, 722 11 Västerås, Sweden
13 Department of Civil Engineering, College of Engineering, University of Diyala, Diyala Coverenoate, Baqubah 32001, Diyala, Iraq; saad123engineer@yahoo.com
*   Correspondence: chaitanay45@gmail.com (C.B.P.); m.scholz@salford.ac.uk (M.S.)

Abstract: The El Nino Southern Oscillation (ENSO) phenomenon is devastating as it negatively impacts global climatic conditions, which can cause extreme events, including floods and droughts, which are harmful to the region's economy. Pakistan is also considered one of the climate change hotspot regions in the world. Therefore, the present study investigates the effect of the ENSO on extreme precipitation events across the Upper Indus Basin. We examined the connections between 11 extreme precipitation indices (EPIs) and two ENSO indicators, the Southern Oscillation Index (SOI) and the Oceanic Niño Index (ONI). This analysis covers both annual and seasonal scales and spans the period from 1971 to 2019. Statistical tests (i.e., Mann–Kendall (MK) and Innovative Trend Analysis (ITA)) were used to observe the variations in the EPIs. The results revealed that the number of Consecutive Dry Days (CDDs) is increasing more than Consecutive Wet Days (CWDs); overall, the EPIs exhibited increasing trends, except for the Rx1 (max. 1-day precipitation) and Rx5 (max. 5-day precipitation) indices. The ENSO indicator ONI is a temperature-related ENSO index. The results further showed that the CDD value has a significant positive correlation with the SOI for most of the UIB (Upper Indus Basin) region, whereas for the CWD value, high elevated stations gave a positive relationship. A significant negative relationship was observed for the lower portion of the UIB. The Rx1 and Rx5 indices were observed to have a negative relationship with the SOI, indicating that El Nino causes heavy rainfall. The R95p (very wet days) and R99p (extreme wet days) indices were observed to have significant negative trends in most of the UIB. In contrast, high elevated stations depicted a significant positive relationship that indicates they are affected by La Nina conditions. The PRCPTOT index exhibited a negative relationship with the SOI, revealing that the El Nino phase causes wet conditions in the UIB. The ONI gave a significant positive relationship

for the UIB region, reinforcing the idea that both indices exhibit more precipitation during El Nino. The above observations imply that while policies are being developed to cope with climate change impacts, the effects of the ENSO should also be considered.

1. Introduction

Pakistan has regularly experienced a variety of meteorological disasters, including droughts and floods [1–3]. Environmental harm, deaths, financial losses, and population displacement were all results of these catastrophes [4–7]. These natural disasters cannot be avoided, but they may be managed well to reduce the risk that people will be exposed to them. The climate variability known as the El Nino Southern Oscillation (ENSO) is responsible for changes in ocean temperatures over the equatorial Pacific. Over time, the ENSO has had a significant influence on the world's climate and weather [8–10]. El Nino, or the warm phase, occurs when the ocean water is noticeably warmer than normal [11–13], and a cold phase, known as La Nina, occurs when the ocean water becomes significantly colder than usual, and it is thought to follow a roughly opposite pattern to that of El Nino [14–16]. Pakistan has had rainfall that has been above or below average at various times during the past few decades due to the ENSO [17–19]. When the ENSO is present, Pakistan has a weather anomaly that impacts both the summer and winter rains [17,18,20]. During El Nino episodes, the summer monsoon rainfall confronts shortfall across Pakistan and can result in meteorological droughts, which are conditions that can happen when precipitation is insufficient to support established human activities [17,19–23]. However, during La Nina years, which often cause floods, it receives near-normal to above-normal rainfall [18,24–26]. El Nino circumstances are frequently followed by La Nina conditions, albeit not always [8,27,28].

The Indus River Basin begins in China's Western Tibetan Plateau (TP), travels across India, reaches Pakistan in the north, and empties into the Arabian Sea in the south [29–31]. Pakistan is primarily an agricultural nation, and 85% of its wheat and rice obtain their water from the Indus River [32]. It is Pakistan's lifeblood [33]. Pakistan stores water from the Indus River at the Tarbela Reservoir for use in agricultural and electricity production. This region is referred to as the Upper Indus Basin (UIB) from its source at the Western TP to this reservoir [34,35]. In the UIB, the temperature changes mostly demonstrate regional and seasonal variability [36–38]. The UIB has previously emphasized differences in precipitation throughout time [39–41]. While the authors of [42] found different results between 1980 and 2006, the authors of ref. Archer et al. [40] found substantial rising trends in the winter, in the summer, and in the annual precipitation over the 1961–1999 period. In addition, ref. [30] noted an increase in precipitation in western UIB between 1995 and 2012. Additionally, higher elevations showed more pronounced decreasing precipitation, as seen in reference [43]. The historical records included in the UIB should be used to evaluate these divergent precipitation reactions seen by various researchers utilizing data from various time periods [44–46]. On the other hand, the regional climate of the UIB is significantly impacted by the North Atlantic Oscillation (NAO), the El Nino Southern Oscillation (ENSO), Indian Ocean Dipole (IOD), and Pacific Decadal Oscillations (PDOs) [47]. The Tmax, Tmin, and precipitation in this area need to be better understood for these four climatic indicators. Here, the NAO serves as a predictor of Atlantic Ocean oscillations (mid-latitude westerlies). The influence indices from the Pacific Oscillations and the Indian Ocean Dipole (IOD) are called the ENSO and PDO, respectively. Strong La Nina conditions in 2010 were linked to Pakistan's floods [48]. In the UIB [40], the authors of ref. [48] found a positive and negative connection between the NAO and the winter and summer precipitation levels, respectively. The winter precipitation level and ENSO linkages were described by the authors of ref. [49], where they discovered a consistent

difference between heavier winter precipitation in El Nino years and condensed early winter precipitation in La Nina years. Additionally, ref. [50] discussed how the NAO affected winter precipitation and how the Southern Oscillation Index (SOl) affected the monsoon in the neighboring Himalayas [51–53]. The Indus River contributes water to the largest irrigation system in the world, providing water for 90% of food production in Pakistan, which furnishes 25% of the country [54,55]. However, the Indus Basin is prone to extreme events, i.e., floods and droughts, due to excess or limited stream flows, which affects the crop yields, and ultimately, the economic development of the country. The purpose of this study is to find the effect of the ENSO on the rainfall in the Upper Indus Region of Pakistan. The biggest impact of the ENSO was observed in Pakistan in the event of the 1998 El Nino, due to which a severe drought was experienced in the country for four years. Similarly, in the 2009 El Nino event, In 2010, a massive flood destroyed Pakistan, resulting in millions of dollars' worth of damage [56]. The primary objective of this research is to find the impact of ENSO on the Upper Indus Basin. To meet the requirement, several objectives include the evaluation of different extreme precipitation indices (EPIs) to analyze the extreme events, and an investigation of the spatiotemporal variations in the EPIs by using an Innovative Trend Analysis (ITA) and the Mann–Kendall test. Also, the phases of the ENSO indices and teleconnections of the ENSO-related index, SOI, with EPIs are analyzed using statistical methods.

2. Materials and Methods

2.1. Study Area and Data Sets

The Upper Indus Basin (UIB) is located at the spatial domain of 33°40′ to 37°12′ N and 70°30′ to 77°30′ E (Figure 1). The Indus Basin is considered to be one of the largest transboundary river basins in the world, shared by different countries including Pakistan (56%), India (26.6%), China (10.7%), and Afghanistan (6.7%) [57]. Due to its large boundary, it is a complex and entangled geopolitical region. It flows through the three mighty mountain ranges, including Karakoram, Hindukush, and the Himalayas, along with the Tibetan Plateau. As these are the highest mountain ranges in the world, they also encompass one of the world's largest glaciated systems, having almost 110,000 glaciers in number [16] with a massive area of about 16,000 km^2 of the surface area [58]. The annual average precipitation distribution varies from 1065 mm to 70 mm with elevation, while going from the direction of southeast to the northwest. The elevation of the area ranges between 8616 m and 140 m from the north to south direction of the UIB [59]. The water supplied by the UIB works as a lifeline for the socio-economic development of the country, and millions of inhabitants depend on it. The water demand in Pakistan is very high due to its utilization in agricultural and hydropower generation divisions; therefore, the Indus Basin is the most overstressed basin in the world [60]. Therefore, it is necessary to study the climatic changes in the UIB as it is considered the lifeline of the country.

2.2. Data Collection

The daily precipitation data were collected from PMD and WAPDA for 12 stations in the UIB. The data ranged from 15 to 49 years as there are some highly elevated areas whose gauge was installed later compared to other stations. The ENSO data including Nino 3.4 and ONI were taken from the Climate Prediction Center (CPC) www.cpc.ncep.noaa.gov (accessed on 12 July 2023). For SOI monthly pressure, data were taken for Tahiti and Darwin for 50 years from Climate Research Unit UK website https://crudata.uea.ac.uk/cru/data/soi/ (accessed on 10 September 2023). For the ONI, monthly and seasonal data were taken for 50 years. For Nino 3.4, 50-year SST data were taken. The stations and their characteristics are shown below in Table 1.
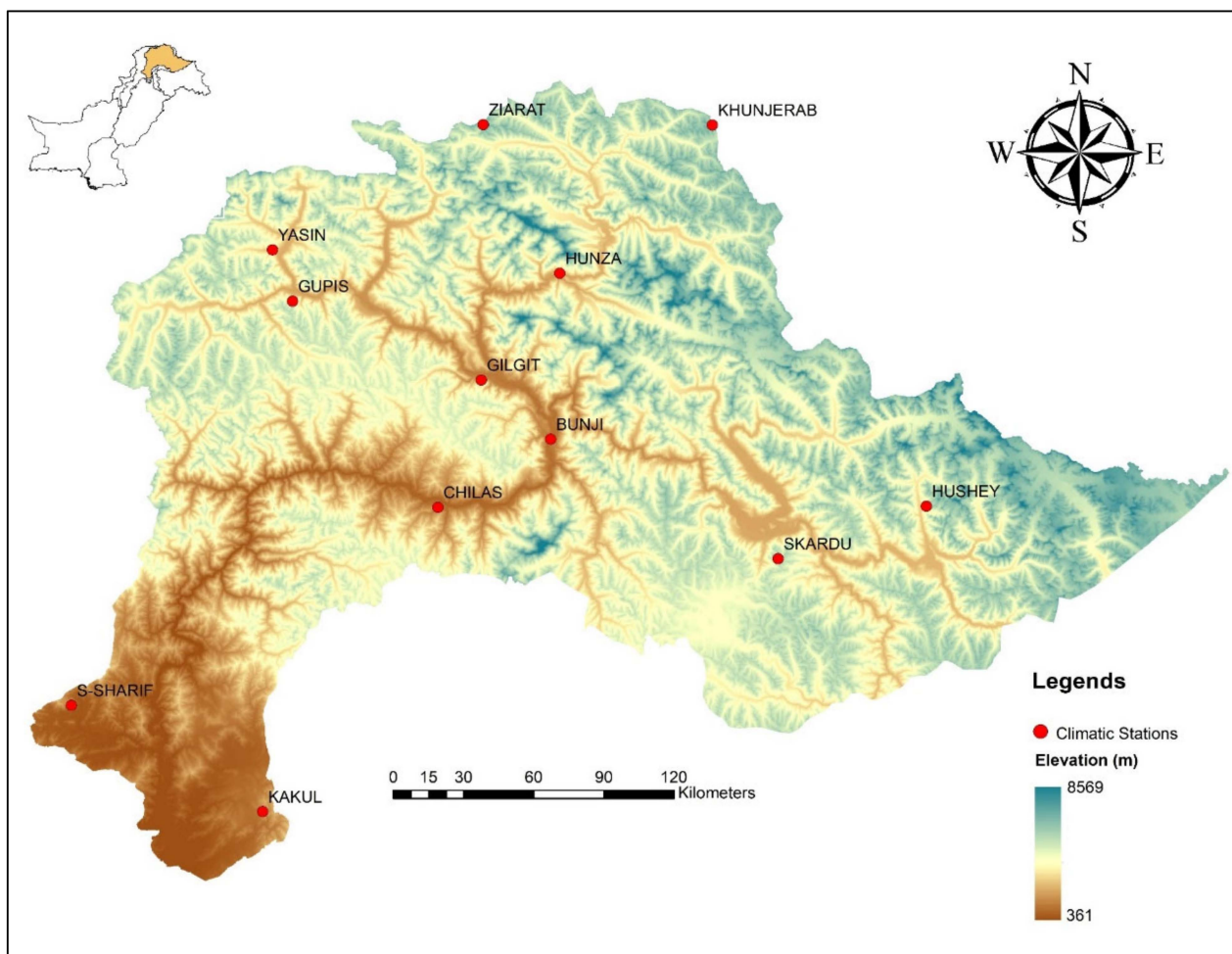
Figure 1. Study area (Upper Indus Basin) with climatic stations and elevation data.

Table 1. List of precipitation gauges.

Sr. No.	Stations	Longitude (Decimal Degrees)	Latitude (Decimal Degrees)	Elevation (m)	Mean Annual Precipitation (mm)	Available Data (Year)
1	Bunji	74.63	35.67	1372	164	1974–2020
2	Chilas	74.1	35.4	1251	215	1980–2020
3	Gilgit	74.3	35.9	1460	134	1975–2020
4	Gupis	73.4	36.2	2156	201	1972–2020
5	Hunza	74.67	36.32	2200	263	2007–2020
6	Hushey	76.4	35.4	3010	526	1995–2020
7	Kakul	73.3	34.2	1309	1242	1971–2020
8	Khunjerab	75.4	36.9	5182	280	1999–2020
9	Skardu	75.7	35.2	2210	237	1971–2020
10	S-Sharif	72.4	34.6	962	957	1974–2020
11	Yasin	73.3	36.4	3353	474	1999–2020
12	Ziarat	74.3	36.9	3688	395	1999–2020

2.3. Precipitation Extreme Indices

The Expert Team on Climate Change Detection and Indices (ETCCDI) standardized 27 extreme indices, out of which 11 indices were related to precipitation [61]. The indices were calculated using the package RClimDex 1.1 in R. The indices used are explained below in Table 2.

Table 2. Extreme precipitation indices recommended by ETCCDI.

Index	Name	Definition	Unit
CDD	Consecutive dry days	Maximum consecutive days having R < 1 mm	days
CWD	Consecutive wet days	Maximum consecutive days having R ≥ 1 mm	days
PRCPTOT	Annual total wet day precipitation	Total precipitation on wet days annually, i.e., R > 1 mm	mm
R10mm	Number of heavy precipitation days	Annual count of days when R ≥ 10 mm for the given period	days
R20mm	Number of very heavy precipitation days	Annual count of days when R ≥ 20 mm for the given period	days
R25mm	Number of extremely heavy precipitation days	Annual count of days when R ≥ 25 mm for the given period	days
R95p	Very wet days	Annual total precipitation when R > 95th percentile where R > 1 mm	mm
R99p	Extremely wet days	Annual total precipitation when R > 99th percentile where R > 1 mm	mm
Rx1 day	Max 1-day precipitation amount	Maximum 1-day precipitation for the given period.	mm
Rx5 day	Max 5-day precipitation amount	Maximum 5-day consecutive precipitation for the given period	mm
SDII	Simple daily precipitation intensity index	Total precipitation divided by the number of rainy days	mm/day

These extreme precipitation indexes are normally used around the world to measure the changes in precipitation patterns [62].

The daily precipitation data should be incorporated into the Excel file in comma-delimited format. The data which are missing are represented by −99.9 or −99.99. Once the file is uploaded, a simple quality control check is performed to find any missing data. The indices are calculated after the QC is performed.

2.4. Spatiotemporal Variation in Indices

To analyze the changes in spatiotemporal variation in extreme precipitation indices, we used the methods described in the methodology flowchart in Figure 2.

2.4.1. Mann–Kendall Test

The Mann–Kendall (M-K) test, also known as the M-K test, is widely used for trend analysis as it is a non-parametric test [63]. A non-parametric test means that the test is unaffected by the normal distribution [64]. The data should not have a serial correlation. If the data have normal distribution, linear regression should be used.

The Mann–Kendall statistics in S are given in the following equation:

$$S = \sum_{k=1}^{n-1} \sum_{j=k+1}^{n} sign(Y_j - Y_k) \tag{1}$$

$$sgn(Y_j - Y_k) = \begin{cases} if\,(Y_j - Y_k) < 0; & then & -1 \\ if\,(Y_j - Y_k) = 0; & then & 0 \\ if\,(Y_j - Y_k) > 0; & then & 1 \end{cases} \tag{2}$$

where Y_j and Y_k = successive data points of time series for the periods j and k, n = the number of data points, and sgn = the function that takes the values −1, 0, 1, as shown above.

The values of S represent the trend; if it is positive, the trend is increasing, and for negative values, it has a decreasing trend. The test is further followed by probability (E) and variance (Var), as suggested by Helsel and Hirsch, as shown below for a sample size of n > 10:

$$E[S] = 0 \tag{3}$$

$$Var(S) = \frac{n(n-1)(2n+5) - \sum_{p=1}^{q} t_p(t_p-1)(2t_p+5)}{18} \tag{4}$$

where q = tied groups, which represent observations of the same value but do not include the location of unique rank numbers, tp = the number of data values in the pth group, and sigma ($\sum$) = the sum of all tied groups.

Figure 2. Schematic diagram of methodology.

However, if the data do not contain any tied classes, this description sequence can be overlooked. The standardized test statistics (Z_{MK}) value is determined using the equation below after manipulating the variance Var(S) from the above equation:

$$Z_{MK} = \begin{cases} \frac{S-1}{\sqrt{VAR(S)}}, & if \quad S > 0 \\ 0, & if \quad S = 0 \\ \frac{S+1}{\sqrt{VAR(S)}}, & if \quad S < 0 \end{cases} \tag{5}$$

The Z value calculates the magnitude of variation and obeys a normal distribution with a variance of "1" and a mean of "0". The null hypothesis, H0, is tested using the test statistics. When Z_{MK} is greater than Z $\alpha/2$, the data series shows a significant trend. At a confidence level of $\alpha = 10\%$, the computed value of Z_{MK} is compared to the usual distribution table of a two-tailed test. The null hypothesis (H0) for no trend is accepted in a two-tailed test if the computed value of Z_{MK} falls between $-Z1-\alpha/2$ and $Z1-\alpha/2$, and

therefore, H1 is rejected. The patterns in the precipitation time series data are calculated at 1%, 5%, and 10% significance levels in this analysis.

2.4.2. Innovative Trend Analysis (ITA)

The trend analysis test, like the MK test, must meet certain criteria before being used, i.e., there should not be a serial correlation in the time series, and a normal distribution of data should not be present. A new method was proposed by Sen [65] that gives results as a graphical representation of trends without having any assumptions in the time series.

The basis of the ITA lies in the fact that if two time series are identical, their plot would be 45° with a 1:1 ratio in a Cartesian plane. The first half of the data is on the *X*-axis, and the second half is on the *Y*-axis. To categorize each half's variance, a sequence of clusters will be used. If all of the data sets in a scatter diagram are on the 45° (1:1) axis, the hydro-meteorological time series data has no trend.

In the first step of calculating the ITA, the data are equally divided into two halves and are arranged in ascending order. The two halves are arranged on the *X* axis and *Y* axis, respectively, and for their classification of the variance, a sequence of clusters is used. The trend is observed by looking at the scatter plot. If the data sets are completely placed on the 45° (1:1) line, it means there is no trend, and if the data points are distributed in the upward or downward portion of the triangular areas, it represents upward and downward trends, respectively. Figure 3 shows the graphical representation of the ITA. The equation used to estimate the magnitude of the trend is given by [66–68].

$$D = \frac{1}{n} \sum_{i=1}^{n} \frac{10(Y_j - Y_i)}{\mu} \tag{6}$$

where D = the trend indicator, n = the number of data values in each subseries, Y_i and Y_j = the first and second subseries data values, respectively, and μ = the first subseries' means. The negative or positive values of D represent a decreasing or increasing pattern, respectively.
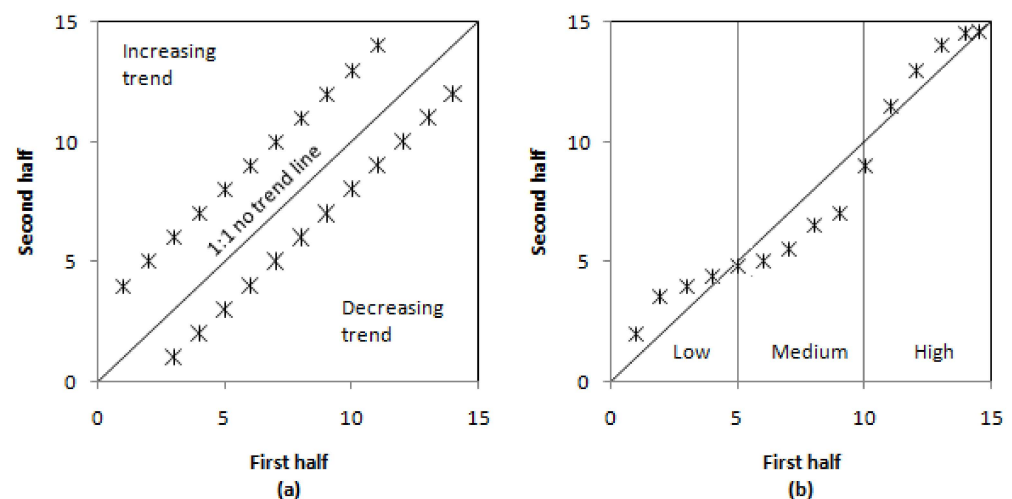
Figure 3. Representation of ITA graph and its components. (**a**) No trend, datasets, (**b**) upward and downward trend, datasets.

2.5. ENSO Index

The ENSO phenomenon, as described above, is a large-scale phenomenon that is observed through atmospheric and sea surface changes. Various indices are used for this purpose; these indices give the overall picture of global circulation patterns that are occurring in the atmosphere and oceanic surface. The index used for this study is mainly the SOI (Southern Oscillation Index). However, other indices are also incorporated to obtain a better picture of the ENSO phenomenon. The purpose of choosing the SOI is that

it has the oldest record for pressure changes from 1866 to the present. Also, it can be used to find the changes in the Walker Circulation and predicts its strength; these changes in the WC further affect the rainfall [69] stream flows, agricultural production, etc.

The Southern Oscillation Index (SOI) mentioned above is a pressure-related index, so it oscillates between two phases known as El Nino and La Nina due to the pressure changes in the Tahiti and Darwin areas. The SOI gives stable values when the Tahiti minus Darwin index is calculated for the global phenomenon. (https://climatedataguide.ucar.edu/climate-data/southern-oscillation-indices-signal-noise-and-tahitidarwin-slp-soi (accessed on 12 July 2023)).

The SOI values move from −1 to 1, indicating El Nino and La Nina conditions, respectively. The threshold for the SOI is −0.5 and 0.5, i.e., if the SOI values go down from −0.5, this indicates an El Nino event, and if they move upward from 0.5, this indicates a La Nina event.

Derivation of SOI

The Southern Oscillation Index is a standardized index, which means its values are confined between −1 and 1 for a better understanding of the phenomenon. The NOAA used a method for calculating the SOI, which is shown below:

$$\text{Tahiti Anomaly} = \text{Actual Sea Level Pressure} - \text{Mean Sea Level Pressure} \tag{7}$$

$$\text{Darwin Anomaly} = \text{Actual Sea Level Pressure} - \text{Mean Sea Level Pressure} \tag{8}$$

The anomalies are calculated by using the climatology of the 1951–1980 period.

$$\text{Tahiti Standard Deviation} = \frac{\sqrt{\sum(\text{Tahiti Anomaly})^2}}{N} \tag{9}$$

$$\text{Darwin Standard Deviation} = \frac{\sqrt{\sum(\text{Darwin Anomaly})^2}}{N} \tag{10}$$

$$\text{Standardized Tahiti} = \frac{\text{Actual SLP} - \text{Mean SLP}}{\text{Standard Deviation Tahiti}} \tag{11}$$

$$\text{Standardized Darwin} = \frac{\text{Actual SLP} - \text{Mean SLP}}{\text{Standard Deviation Darwin}} \tag{12}$$

$$\text{MSD} = \frac{\sqrt{\sum(\text{Std. Tahiti} - \text{Std.Darwin})^2}}{N} \tag{13}$$

$$\text{SOI} = \frac{\text{Std. Tahiti} - \text{Std. Darwin}}{\text{MSD}} \tag{14}$$

2.6. Oceanic ENSO Indices

The ENSO comprises atmospheric as well as oceanic temperature indices. For this purpose, other indices dealing with sea surface temperature (SST) were also used, named Nino 3.4 SST and ONI.

For the sea surface temperatures, different regions are considered in the Pacific. These regions are termed Nino 1 + 2, Nino 3, Nino 3.4, and Nino 4. The locations of these regions are shown below in Table 3 and Figure 4.

For the current study, the Nino 3.4 SST Index is used. The Nino 3.4 Index uses a 5-month running mean, and El Nino and La Nina are considered when the Nino 3.4 SSTs exceed ±0.4 °C for six months or more.

The ONI is known as the Oceanic Nino Index, which uses the same region as Nino 3.4: 5 N-5 S, 170 W-120 W. The ONI uses a three-month running mean, and for El Nino or La Nina events, the anomalies must exceed ±0.5 °C for at least 5 consecutive months. It is defined by NOAA.

Table 3. Nino types.

SST Region	Location	Comments
Nino 1 + 2	0-10 S, 90 W-80 W	It is the most eastern part of Nino SST and is also the smallest.
Nino 3	5 N-5 S, 150 W-90 W	It was considered as the key region for ENSO but it was observed that the key region lies further in the west [70].
Nino 3.4	5 N-5 S, 170 W-120 W	SST anomalies for this region are considered average for the Pacific Ocean
Niño 4	5 N-5 S, 160 E-150 W	Nino 4 index captures SST anomalies in the central equatorial Pacific. It has less variance than the other SST regions.
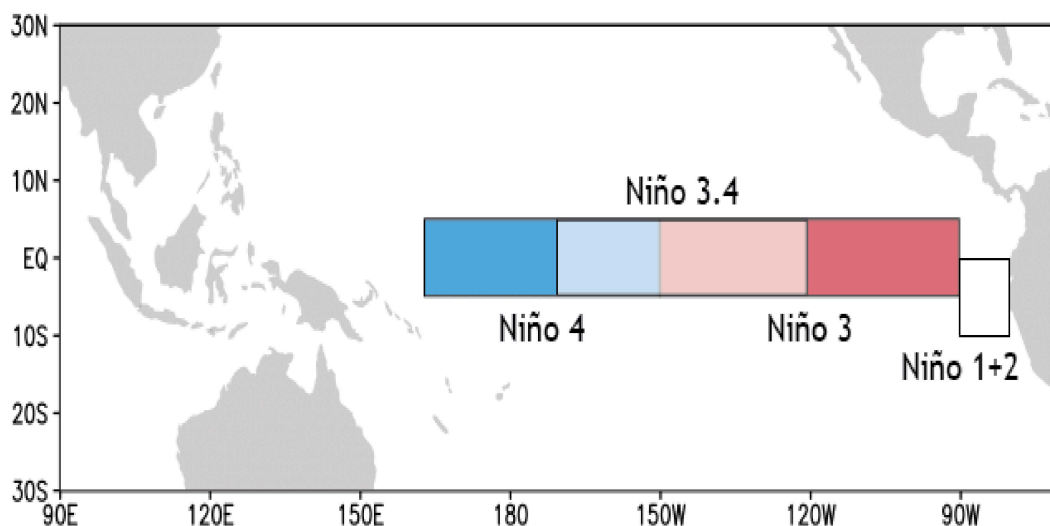
Figure 4. Sea surface temperature regions in the Pacific Ocean.

2.7. Teleconnections of ENSO

Teleconnections deal with large-scale atmospheric changes that occur globally. These patterns occur from weeks to months and can extend even to years. ENSO teleconnections mean that a change in one part of the globe can affect the other regions of the world.

The teleconnections of the SOI are found on annual and seasonal bases. For the annual time series, the SOI averaged values are calculated annually, and for seasonal values, 3-month averages are used to find 4 seasons denoted as DJF, MAM, JJA, and SON. The annual and seasonal SOI values are lagged and related to EPIs using the Pearson Correlation Method to find the Pearson coefficient. The correlation coefficient is further elaborated by finding the *p*-value [71].

Pearson Correlation Method

The Pearson Correlation Method, also known as the Pearson Product Moment Correlation Method, is used to find how much two variables are related to each other. The formula used for the Pearson Correlation Method is shown below:

$$r = \frac{\sum (x_i - \bar{x})(y_i - \bar{y})}{\sqrt{\sum (x_i - \bar{x})^2 \sum (y_i - \bar{y})^2}} \quad (15)$$

The Pearson Correlation Method is a widely used method for finding relationships between two entities. The Pearson coefficient ranges from −1 to 1, and it shows how strong or weak the relationship between two variables is; −1 shows that the two variables are inversely related, and +1 shows that the variables are positively related. The values near ±0.5 give a good correlation value. The Pearson correlation coefficient is further elaborated using a *p*-value. The *p*-value shows the significance of the relationship; if $p < 0.05$, it means the relationship is significant, and there is a strong probability of one variable affecting the other.

3. Results and Discussion

3.1. Spatiotemporal Variations in Precipitation over the Upper Indus Basin

The Upper Indus Basin is a complex region as it is affected by different climatic phenomena occurring in different regions. It can be seen that due to these climatic effects, such as monsoons, westerly winds, and orographic variations, there is a large variation in the precipitation of the Upper Indus Basin.

By observing the 12 stations in the UIB, it is seen that the variation in the monthly time series is not that significant. However, higher than average precipitation can be observed in the months of July and August, with about 40% more precipitation than in other months; this is because they lie in the monsoon period, as precipitation mainly occurs during the monsoon in Pakistan. Along with the monsoon effect on precipitation, an increase in precipitation is also observed from February to April; this can be attributed to the climate change that increases the temperature in the UIB, and abrupt changes are observed in the spring season, as discussed in [72].

Looking at the variation in the annual time series, a much larger diversification is observed compared to the monthly variation. This can be due to several reasons. As we know, the UIB is affected by different climate phenomena, such as monsoons and westerly winds, and orographic variations in different areas [73]. The monsoon is the main regime that causes precipitation in the country, and it is observed that the stations of Kakul and Saidu Sharif lie in the particular area of monsoons, due to which they depict high precipitation levels with increases of 60% and 56%, respectively, than the average precipitation levels of other stations. The stations in the northwest part of the Upper Indus Basin, like Ziarat and Yasin, displayed 10% more average precipitation than the stations situated between the Karakoram and Himalayas areas. This can be due to the effect of westerly disturbances that cause little precipitation. The stations situated between the Karakoram and Himalayas areas, such as Gilgit, Bunji, and Chilas, depicted the lowest precipitation, having 38%, 52%, and 35%, respectively, less precipitation than the average, which can be attributed to the orographic deviations that cause the least precipitation. Figure 5 shows the spatial mean annual variation in the Upper Indus Basin. Figures 6 and 7 show the temporal mean annual variation and the mean monthly variation, respectively.
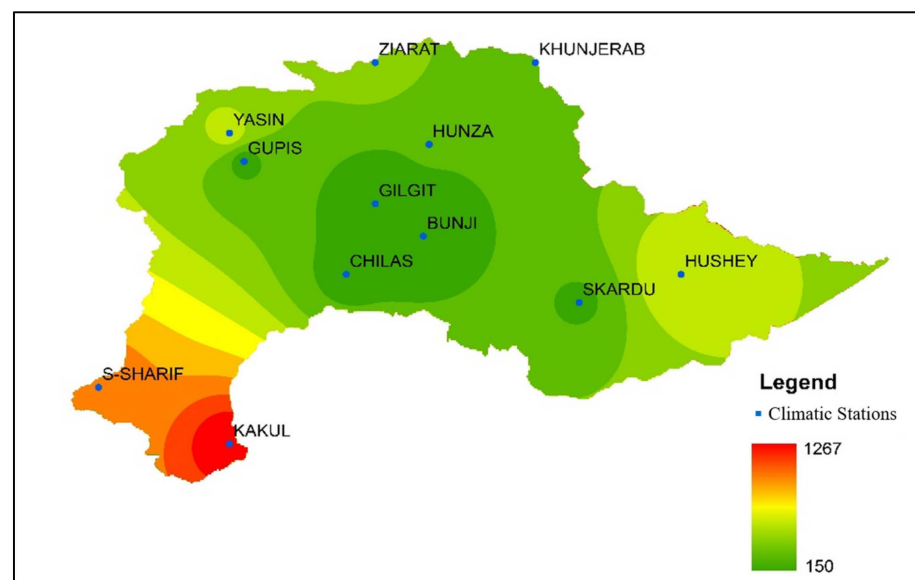
Figure 5. Spatial mean annual variation (mm).
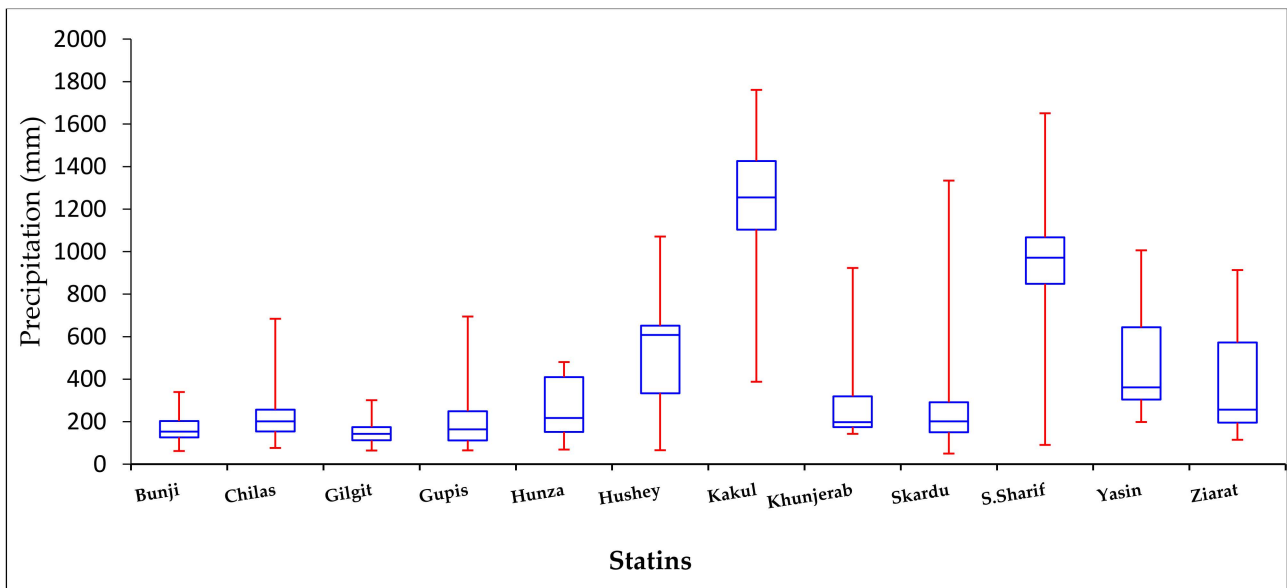
Figure 6. Temporal mean annual variation.
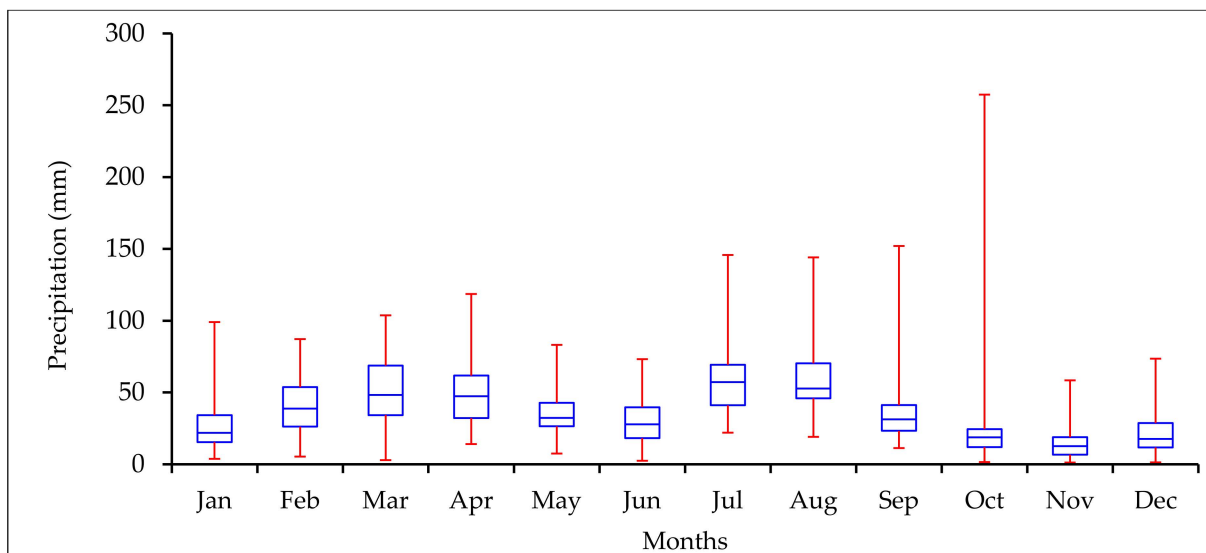
Figure 7. Temporal mean monthly variation.

3.2. Spatiotemporal Variation in EPI

The spatiotemporal variations are examined in the extreme precipitation indices (EPIs) using statistical methods. It is observed that both significant increasing and decreasing trends are displayed by different EPIs in the Upper Indus Basin. For most of the EPIs, two stations, Yasin and Ziarat, showed increasing trends. The total precipitation index (PRCPTOT), R10mm, R20mm, and R25mm gave significantly increasing trends for almost all of the stations, but three stations, Chilas, Kakul, and Skardu, gave decreasing trends.

The magnitude for PRCPTOT was found to be 5.23 mm/year, which shows an overall increase in precipitation. The index presented increasing and decreasing trends for nine and three stations, significant increasing trends were observed for six stations, and significant decreasing trends were observed for two stations (Chilas and Kakul), depicting an overall increase in precipitation.

The heavy precipitation days indices (R10mm, R20mm, and R25mm) had increasing magnitudes with the rates of 0.06 mm/year, 0.02 mm/year, and 0.00 mm/year. For the increased heavy precipitation indices, it was seen that the magnitude of precipitation

was decreasing. R10mm and R25mm exhibited decreasing trends for eight stations and increasing trends for four stations, with significant increasing trends for two stations (Khunjerab and Ziarat). R20mm presented decreasing trends for seven stations and increasing trends for five stations, with significantly increasing trends for two stations (Khunjerab and Ziarat).

Indices like the CDD and CWD both gave significantly increasing results for four stations and significantly decreasing results at one station, which is Hushey. The magnitudes of CDD and CWD were 0.13 days/year and 0.09 days/year, respectively. As CDD was increasing more than CWD, dry conditions were the most likely to be observed.

R95p and R99p both had increasing magnitudes of 0.11 mm/year and 0.08 mm/year, but they both had decreasing trends for eight stations and increasing trends for four stations. The indices displayed that five stations had significantly decreasing trends. Hunza and Hushey both had significantly decreasing trends for R95p and R99p.

The Rx1 and Rx5 (maximum 1 and 5-day precipitation) indices presented decreasing and increasing trends for eight and four stations, respectively. A significant increasing trend was observed for only two stations, Khunjerab and Ziarat, and a significantly decreasing trend was only observed for Hushey. The indices were decreasing at the rates of 0.08 mm/year and 0.05 mm/year, respectively.

Along with the Rx1 and Rx5 indices, the SDII exhibited decreasing and increasing trends for nine and three stations, respectively, with significant decreasing trends for seven stations, and two stations displayed significantly positive trends, including Khunjerab and Ziarat. The magnitude of the SDII was found to be decreasing at the rate of 0.02 mm/day/year. The spatial patterns of the extreme precipitation indices are shown in Figure 8. The graphical representation of the ITA is shown in Figures A1–A10 in Appendix A. Most stations are within 10% variation of the (1:1) line of ITA. Some anomalous values were also observed, which were not included in the variance.
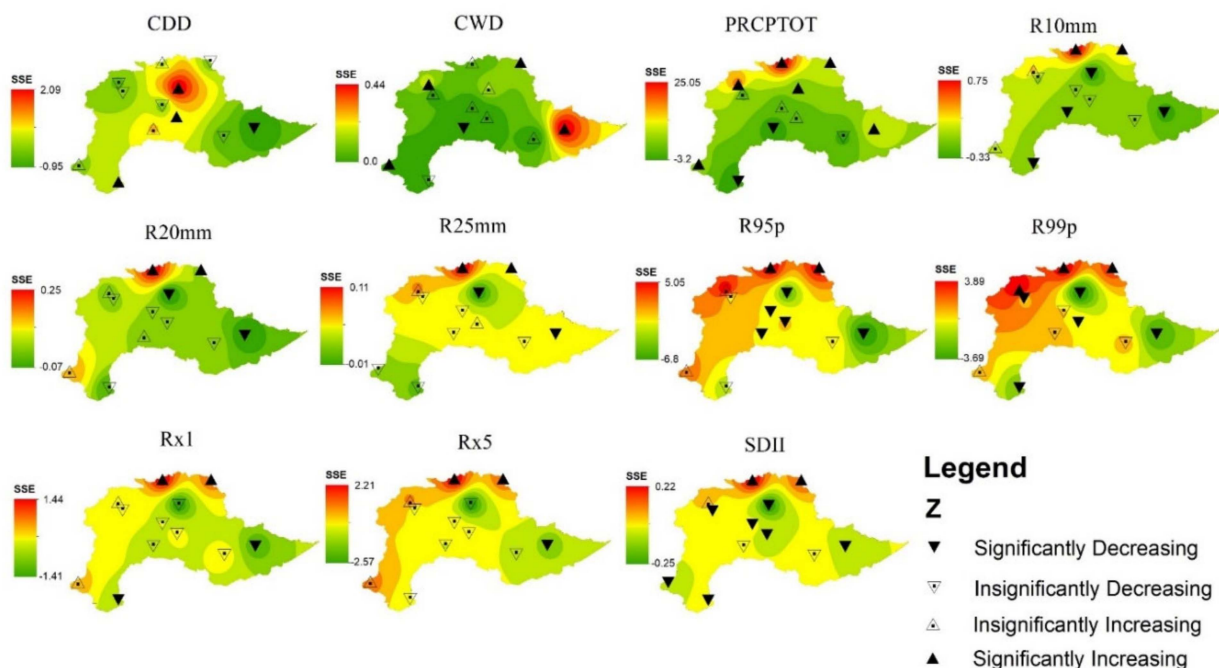
Figure 8. Spatial patterns of extreme precipitation indices in the Upper Indus Basin.

3.3. Comparison of MK and ITA

The results of the MK test and ITA are graphically represented by radial graphs in Figure 9. By analyzing the trends of both the MK test and ITA, it was observed that out of 132 time series, 47% and 52% of the trends were significant for the MK test and ITA, respectively. The results for almost all of the EPIs are comparable with very little difference.

While analyzing the CDD values, it was observed that both had the same number of significant trends, but there was little difference in the overall trends. The MK test showed six stations with increasing and decreasing trends, whereas one station (Hushey) indicated a significantly decreasing trend. The ITA, on the other hand, had four and eight stations depicting decreasing and increasing trends, respectively. In the case of the CWD value, 10 stations had increasing trends and 2 stations had decreasing trends for the MK test, while the ITA had 9 stations showing increasing trends and 3 stations showing decreasing trends. Four stations, including Hushey, Khunjerab, Saidu Sharif, and Yasin, showed significantly increasing trends for the MK test, and five stations, including Hunza, Hushey, Khunjerab, Yasin, and Ziarat, exhibited significant positive trends for the ITA. Only one station (Chilas) showed a significantly decreasing trend for the MK test, and none were observed for the ITA.
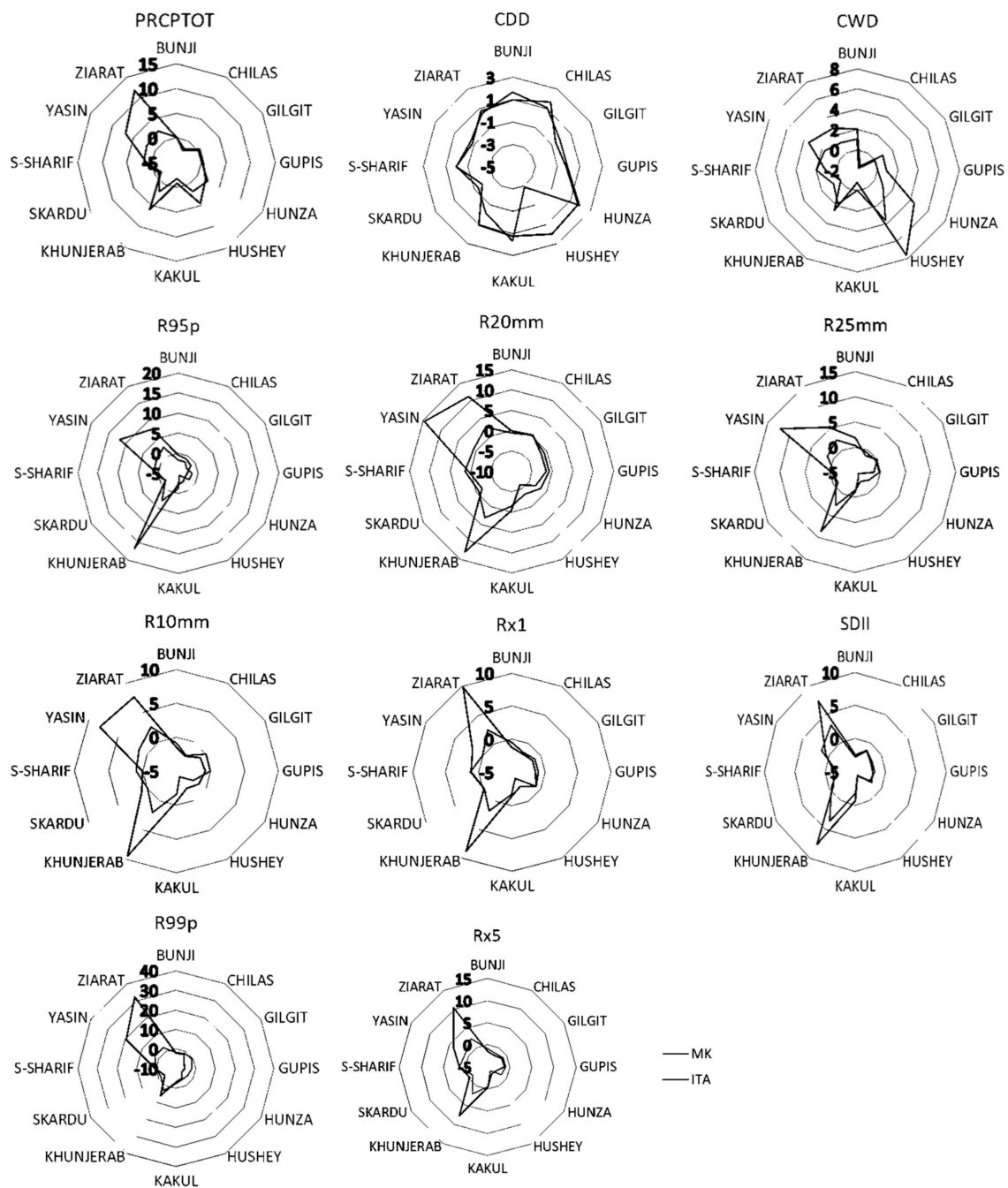
Figure 9. Radial graph representing MK test and ITA comparison.

PRCPTOT, R95p, R99p, Rx1, Rx5, and SDII gave exact increasing and decreasing trends for the MK test and ITA, with a small difference in the significant trends. In the case of PCPTOT, six stations exhibited significantly increasing trends, and two showed significantly decreasing trends, while the ITA had five stations exhibiting significantly increasing trends and only one station with a significantly decreasing trend. Hunza, Hushey, Khunjerab, Yasin, and Ziarat exhibited significantly increasing trends in both the MK test and ITA. The statistical tests indicate that Chilas manifested a decreasing trend for PRCPTOT.

While investigating the R10mm, R20mm, and R25mm indices, it was found that two stations gave significantly increasing trends for the MK test, including Khunjerab and Ziarat. In the case of the ITA, along with the aforementioned stations, Yasin also displayed a significantly positive trend. Hushey was the common station in the very heavy precipitation days indices that gave significantly decreasing trends for both the MK test and ITA.

The percentile indices, R95p and R99p, also depicted similar results for both the MK test and ITA, with eight stations presenting decreasing trends and four stations presenting increasing trends. Khunjerab, Ziarat, and Yasin showed significantly increasing trends for both the MK test and ITA, and Hunza and Hushey, along with Gilgit, exhibited significantly decreasing trends for both the MK test and ITA and for both percentile indices. Similarly, the maximum number of heavy precipitation days indices, i.e., Rx1 and Rx5, displayed comparable results, with eight stations showing decreasing trends and four stations showing increasing trends. Khunjerab and Ziarat showed significantly increasing trends, and Hushey and Hunza, along with Chilas, showed significantly decreasing trends.

The SDII index, on the other hand, exhibited nine stations with decreasing trends, and only three stations depicting increasing trends for both statistical tests, out of which only two stations, Khunjerab and Ziarat, exhibited significantly increasing trends. In the case of the MK test, seven stations displayed significantly decreasing trends, whereas five stations depicted significantly decreasing trends. The common stations depicting significantly decreasing trends consisted of the Hunza, Hushey, and Gilgit stations. It was seen that some of the stations, like Khunjerab and Ziarat, showed significantly increasing results for the maximum cases; this might be due to the stations being highly elevated. Other stations like Gilgit, Hushey, and Hunza showed significantly negative trends; this is similar to what was observed in [74]. The overall results reveal the compatibility between the MK test and ITA, but a difference was observed due to the nature of the two statistical tests. The MK test does not consider outliers while evaluating trends, whereas the ITA considers the outliers during the evaluation. The ITA has the ability to distribute the data into low, median, and high values, whereas the MK test has limitations such as the natural distribution of data, it and should be independent of any correlations.

3.4. Comparison of ENSO Indices

The ENSO indices are compared to one another, revealing that the ONI index exhibits contrasting relationships. For El Niño events, the ONI values are positive, whereas during La Niña events, the ONI values become negative. This relationship is consistent with the SST indices, as both are calculated for the same Nino 3.4 region. It is shown below in Figure 10.

3.5. Phase Identification

The phase of Nino 3.4 is found by calculating the 5-month running mean, and for the ONI, the 3-month running mean is considered. For the SOI average, the seasonal value is considered for the phase identification. The phase for the ENSO year is considered when the atmospheric and temperature indices give an El Nino, neutral, or La Nina phase. As it is known that the ENSO is a complex global phenomenon, it is better to observe the behaviors of different ENSO indices to identify the phase of the ENSO. The climatic departments of the world have a consensus that strong El Nino events occurred in 1982, 1983, 1997, 1998, 2015, and 2016, whereas strong La Nina events were observed in the years 1973, 1974, 1975,

1976, 1988, 1989, 1998, 1999, 2000, 2007, 2008, 2010, and 2011. The phases observed in the study also verify the phases of the ENSO. The graph below shows the different years of El Nino, La Nina, and neutral years for the SOI and ONI (Figure 11).
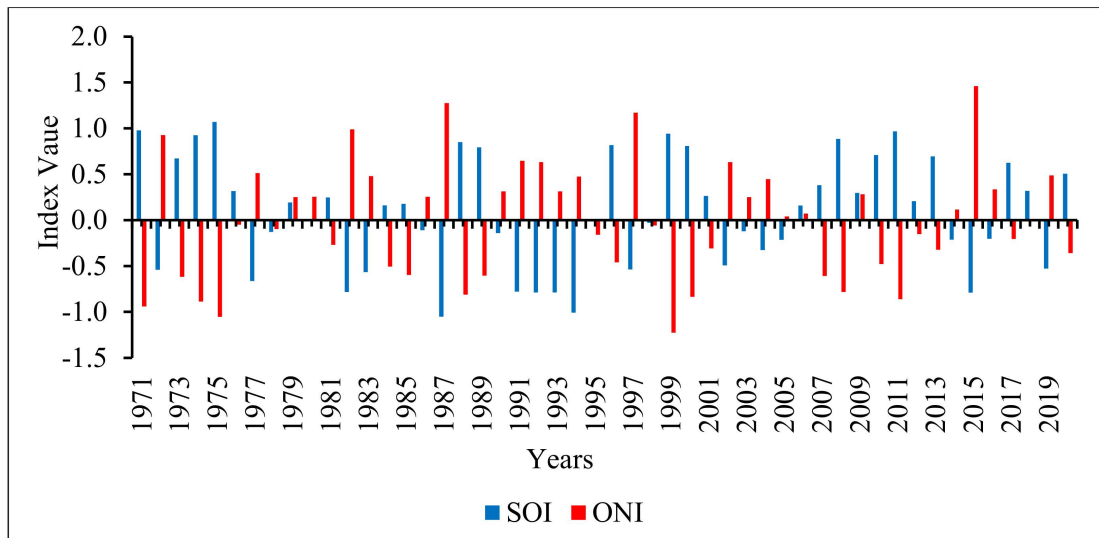
Figure 10. Comparison of SOI vs. ONI.
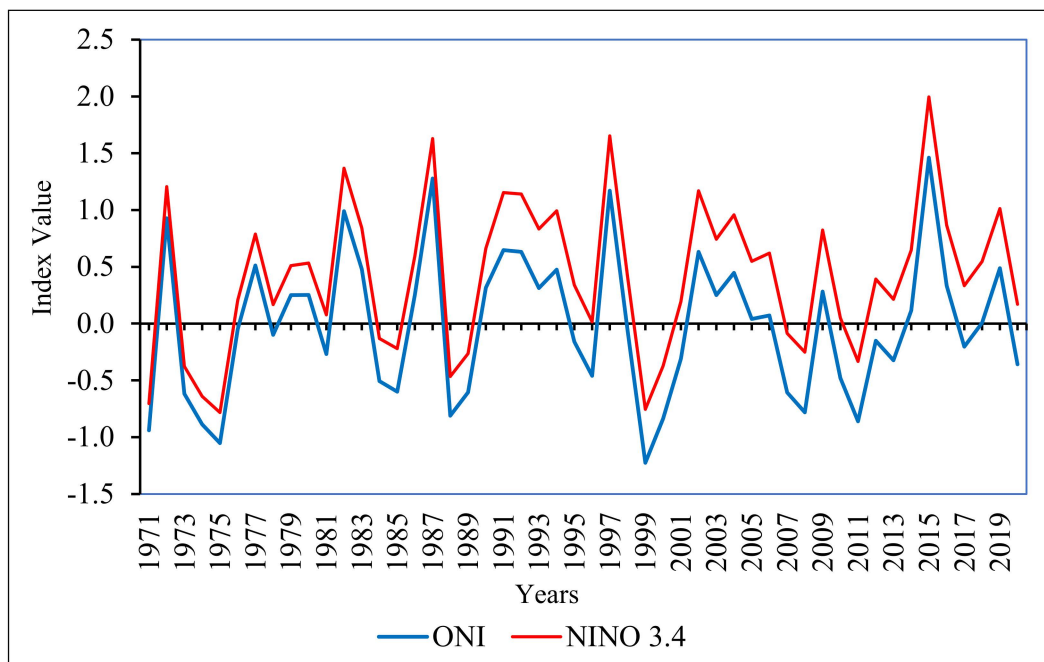
Figure 11. Comparison of ONI vs. NINO 3.4.

3.6. Precipitation Trend during ENSO Phase in UIB

A general pattern of precipitation was observed for 50 years in the UIB during different phases of the ENSO, and it exhibited that from 15 La Nina events occurring in 50 years with respect to the SOI, 8 events increased the average precipitation, with the index value of maximum increase being 0.6. Out of 13 El Nino events, on the other hand, 10 events increased the precipitation from the average, with the minimum increase being 0.1 and the maximum increase being 0.6 (Figure 12). By analyzing the ONI events for the UIB, it was observed that 10 out of 15 El Nino events increased the precipitation, with the maximum increase of 1 in the index, and a minimum increase of 0.1, and 6 out of 15 La Nina events

increased the precipitation, with the maximum increase in the index value being 0.7, and the minimum index value being 0.1 (Figures 13 and 14). The pattern revealed that the increase in precipitation occurred during the El Nino phase of the ENSO (Figure 15), and decreased precipitation was observed during the La Nina phase of the ENSO [75].
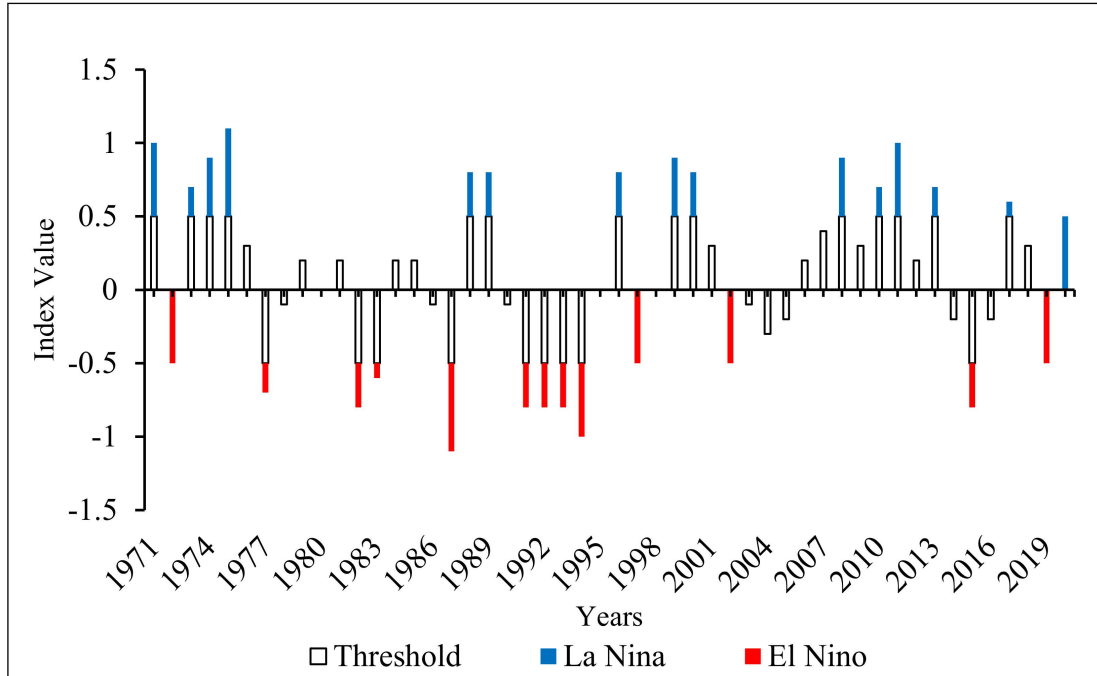
Figure 12. ENSO phases in SOI in the 1971–2020 period.
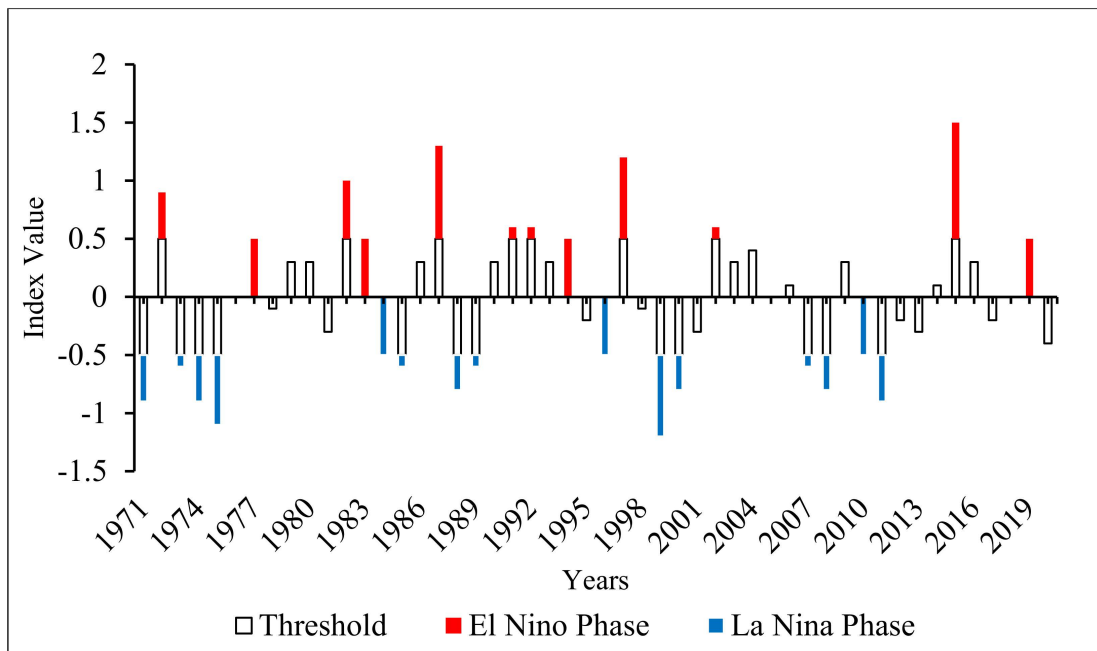
Figure 13. ENSO phases in ONI in the 1971–2020 period.
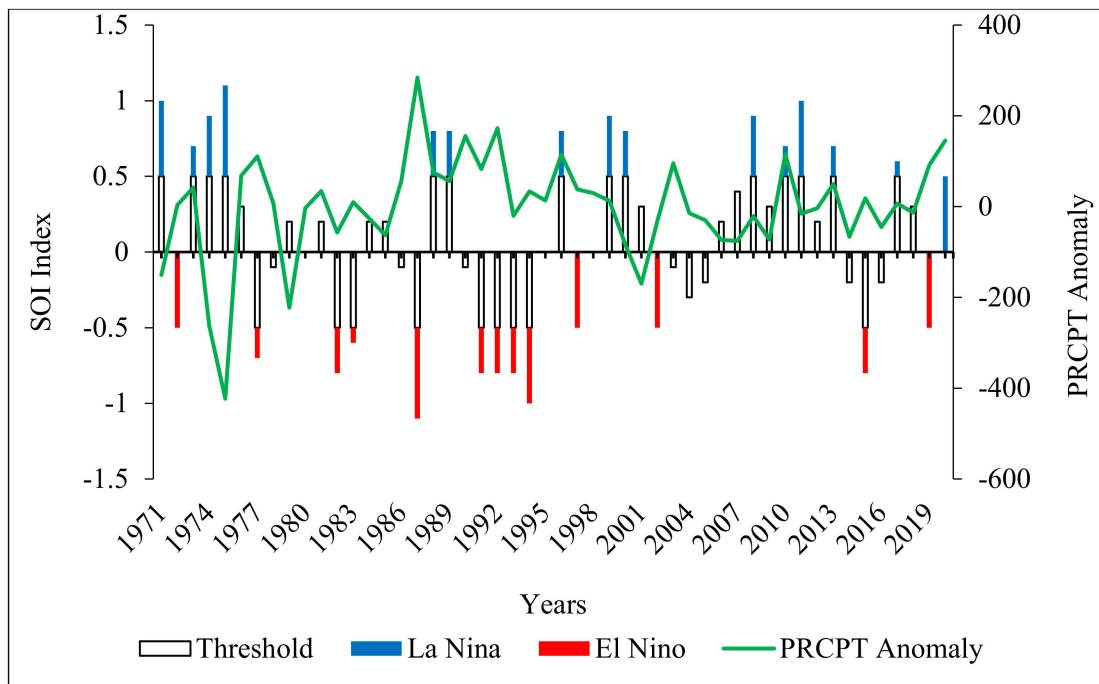
Figure 14. Precipitation in UIB during ENSO phases of SOI.
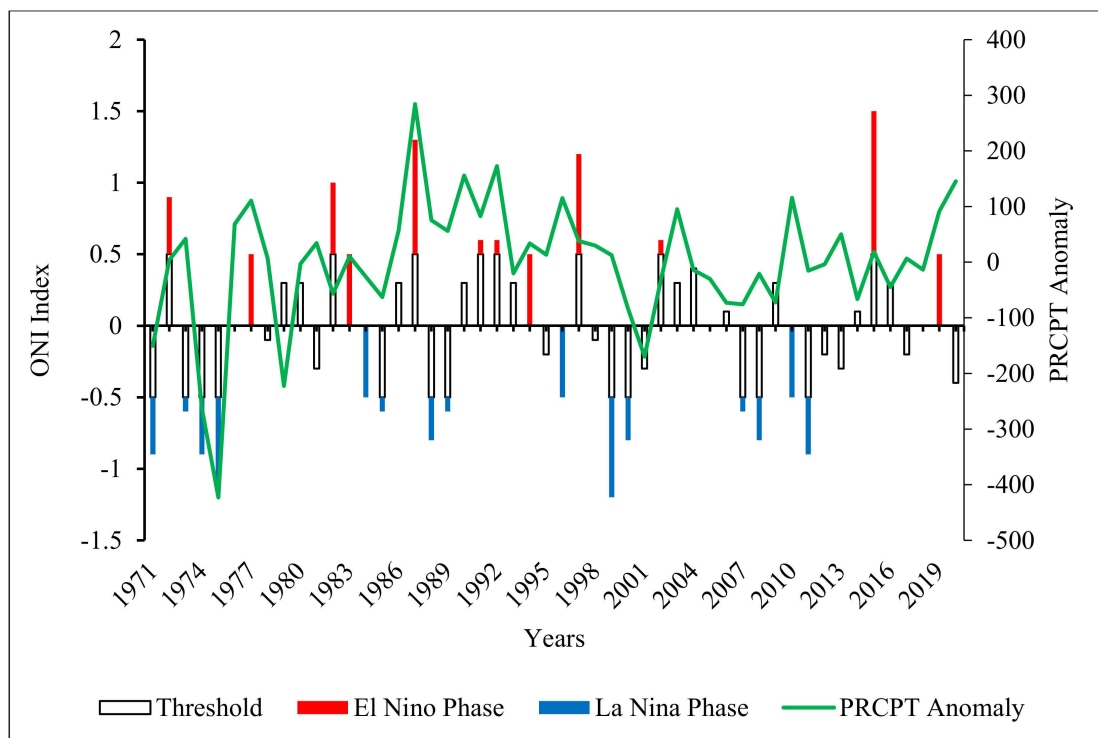
Figure 15. Precipitation in UIB during ENSO phases of ONI.

3.7. Correlation of ENSO Indices and EPIs

3.7.1. Annual Scale Correlations

Teleconnections between the ENSO indices and EPIs were analyzed using the Pearson Correlation Method. The seasonal and annual time series of the SOI and ONI were used to find the relationship between the ENSO indices and extreme precipitation indices (EPIs). For the annual time series, considering the CDD index, it was observed that five stations, Hunza, Hushey, Khunjerab, Kakul, and Gupis, were negatively correlated with the SOI,

and the remaining seven stations were positively correlated with the SOI. In the case of the ONI, four of the above stations, Gupis, Hunza, Hushey, and Kakul, showed positive correlations, but Khunjerab showed anomalous behavior by exhibiting a positive correlation with the ONI. This might be due to Khunjerab being a highly elevated area, and it might be affected by La Nina conditions more than El Nino conditions. The other seven stations had a negative correlation with the ONI, depicting increases in dry days during the El Nino period.

In the case of the CWD index, inconsistent behavior was observed, as eight stations were positively correlated and four were negatively correlated with the SOI. The central stations of the region had a negative correlation, including the Gupis, Chilas, Hunza, and Bunji stations, while the other stations showed significant positive relationships with the SOI. While the ONI showed an opposite result, eight stations were negatively correlated, while four stations were positively correlated with the ONI. It was also seen that Bunji, Chilas, and Hunza depicted the same behaviors and had positive correlations with the ONI, showing that the precipitation in these central stations of the UIB increases during the El Nino phase.

While investigating the PRCPTOT index, six stations, Bunji, Chilas, Gupis, Hunza, Kakul, and Skardu, depicted negative correlations, in which three stations, Chilas, Gupis, and Hunza, had significant negative relationships with the PRCPTOT, and the remaining six stations had positive correlations, of which three stations, Khunjerab, Hushey, and Yasin, were significantly correlated with the SOI. On the other hand, the ONI also gave similar results, but four stations (Gilgit, Hunza, Hushey, and Khunjerab) had significant negative correlations, and two stations (Chilas and Gupis) had significant positive correlations.

The very heavy precipitation days indices show similar trends, with most stations having negative correlations with the SOI, and with Gupis and Hushey showing significant negative correlations with R10mm, R20mm, and R25mm. For the ONI Bunji, Hushey, Kakul, Khunjerab, and Saidu Sharif had positive correlations, but no significant correlation was found.

The extremely wet days indices (R95p and R99p) gave similar results, with five stations showing positive correlations, and seven stations showing negative correlations with the SOI. Gilgit, Gupis, and Hushey showed significant negative correlations, while Hunza, Yasin, and Ziarat showed significant positive correlations with the SOI. In the case of the ONI, Chilas and Skardu had positive significant results, while Yasin and Ziarat had significant negative correlations.

For the maximum 1-day and 5-day precipitation indices, Chilas, Gilgit, Gupis, Hushey, and Kakul had significant negative correlations with the SOI, and Hunza, Yasin, and Ziarat had significant positive correlations with the SOI. While investigating the ONI correlations with Rx1 and Rx5, it was found that Chilas, Gilgit, Gupis, Kakul, and Skardu had significant positive correlations, whereas Hunza had a significant negative correlation.

The SDII index had a negative correlation with the SOI for nine stations and a positive correlation with three stations. Chilas, Gupis, and Kakul had significant negative correlations, and no positive significant correlation was found. While observing the correlation with the ONI, heterogeneous results were found. Chilas and Skardu had significant positive correlations, while only Hunza had a significant negative relationship with the ONI.

R99p, Rx1, Rx5, and SDII consistently depicted significantly negative correlations for most of the stations in the annual time series for the SOI. These indices indicate an increase during the El Nino phase. Chilas, Gupis, and Hunza, the central areas of the UIB, exhibited increases in precipitation during the El Nino phase of the ENSO. Kakul also presented increased precipitation in the El Nino phase, whereas the high elevated areas like Khunjerab, Yasin, and Ziarat depicted increased precipitation in the La Nina phase of the ENSO; this might be because these stations have very high elevations that can cause the circulation of winds to change and increase precipitation during the La Nina phase. The ONI had a positive correlation, and the SOI had a negative correlation for most of the EPIs, and the same behavior was depicted in the Poyang Lake Basin in China [76].

3.7.2. Seasonal Scale Correlations

The investigation of the springtime series (MAM) relationship between the ENSO and EPIs exhibited almost the same pattern as the annual time series. The CDD index had heterogeneous results with Chilas, Gilgit, and Gupis, exhibiting a positive significant correlation with the SOI, and Hunza, Hushey, Yasin, and Ziarat showed negative significant correlations with the SOI. In the event of the ONI, mixed results were observed for the stations, but three stations, Gupis, Hunza, and Ziarat had significant positive correlations, and Gilgit had a significant negative correlation with the ONI. The CWD index had a negative correlation with the SOI for eight stations, and a positive correlation for four stations. Khunjerab, Skardu, and Ziarat had significant negative correlations with the SOI. Considering the correlation with the ONI, it was observed that nine stations were positively correlated, and three stations were negatively correlated with the ONI. Bunji, Kakul, Saidu Sharif, and Ziarat depicted significant positive correlations with the ONI.

For PRCPTOT, a negative relationship with the SOI was observed for nine stations, and three stations had negative correlations for the SOI in the UIB. Chilas, Gupis, Hunza, Kakul, and Saidu Sharif represented significant negative correlations with the SOI, while Hushey presented a significant positive correlation with the SOI. While investigating the correlation with the ONI, a noteworthy relationship was found, as 11 stations had positive relationships, and only Gilgit presented a negative correlation. Bunji, Gupis, Kakul, Khunjerab, Skardu, Saidu Sharif, and Ziarat had significant positive correlations, enforcing the idea that an increase in precipitation is observed during the El Nino phase of the ENSO.

R10mm, R20mm, and R25mm gave similar results, with maximum stations having negative correlations with the SOI. Gupis and Saidu Sharif displayed negative significant relationships for R10mm and R25mm. For the ONI and R10mm, nine stations presented positive correlations, and three presented negative correlations. Bunji, Hushey, Kakul, Khunjerab, Saidu Sharif, Yasin, and Ziarat exhibited positive significant correlations. R20mm and R25mm did not have significant correlations; however, R20mm showed peculiar behavior, as seven stations were negatively correlated, and four stations were positively correlated with the ONI, which is different from the other heavy precipitation days indices, and this was also in contrast to the results that were examined in California [77].

R95p and R99p had negative correlations with the SOI for seven and eight stations, with Gupis and Hushey having significant negative correlations, and Chilas and Ziarat exhibiting positive significant correlations with the SOI. When analyzing the correlation for the ONI, it was found that heterogeneous observations were conducted for the whole region, with Gupis, Hushey, and Khunjerab presenting significant positive correlations, and Chilas having a significant negative correlation with the ONI.

For Rx1 and Rx5, most stations presented negative correlations with the SOI; Chilas, Gupis, and Hushey had significant negative correlations, whereas no positive significant relationship was found. While observing the correlation for the ONI, it was found that Rx1 gave anomalous results, as most of the stations had negative correlations with the ONI, and only Gupis exhibited a significant positive correlation. Moreover, Rx5 had a positive correlation with nine stations, and Gupis, Hushey, and Khunjerab had significant positive correlations with the ONI. The SDII displayed a substantial correlation, with 10 stations having negative correlations, and 2 stations having negative correlations with the SOI. Bunji and Hushey had significant negative correlation with the SOI, while for the ONI, Hushey, Yasin, and Ziarat presented significant positive correlations.

When analyzing the results exhibited by the stations, it was observed that the central stations, Gupis, Hunza, and Chilas, are well correlated with the SOI and ONI. The monsoon region stations, i.e., Kakul and Saidu Sharif, also exhibited good relationships with the ENSO indices in the springtime series. The highly elevated stations, including Khunjerab, Yasin, and Ziarat, presented heterogeneous behavior with the ENSO indices. This was also observed in [78], where reduced precipitation was observed in highly elevated areas. Considering the summertime series (JJA) for the SOI, a constant pattern was represented for PRCPTOT, and the R10mm, R95p, and Rx1 EPIs had positive correlations with five

stations and negative correlations for seven stations, with Gupis and Hunza exhibiting significant negative correlations, whereas no significant positive correlation was found in any stations for the SOI.

The CDD index had a significant negative relationship with five stations and a significant positive relationship with two stations. However, the SDII had an abnormal pattern, as seen in the annual and springtime series, and it had positive relationships with most of the stations but had significant negative relationships with two stations, with no positive significant trend. The ONI gave significantly positive correlation values for the maximum stations, showing an opposite trend with the SOI. When analyzing the stations of the study area, it can be seen that Hunza and Gupis are stations that give significant results for the ENSO indices, implementing a precipitation increase in the central region of the UIB, whereas no significant correlations were found for the La Nina conditions in the UIB. Furthermore, the pattern of summer rainfall is more aggressive, which might be due to the fact that monsoons also play roles in the summer (JJA), increasing the significant positive trends with the ONI and negative trends with the SOI.

For the Autumn Time Series (SON), the R10mm, R20mm, and Rx1 EPIs had positive correlations with three stations and negative correlations with nine stations, with very few significant trends for one or two stations. The other EPIs also exhibited similar results, with mostly negative correlations with the SOI, but very few significant trends. When investigating the ONI teleconnections, aggressive significant positive correlations were observed. PRCPTOT, R25mm, and R95p had positive correlations for all of the regions, with significant positive relations at five to eight stations. For the SDII, 10 stations showed positive trends, with 5 of them being significant. The overall autumn phase corresponded to JJA aggressively like the Indonesian region [79].

When analyzing the winter time series (DJF) for the SOI, significant trends were found between the CDD and SOI, with eight stations having negative significant correlations. The results depict dry conditions during the El Nino conditions; this, too, corresponds to the DJF behavior in the Indonesian region [79].

R10mm and R99p showed abnormal trends, with positive correlations for maximum stations depicting that these extremes were decreasing with a decreasing SOI, i.e., the El Nino phase is reducing the extremes, and the La Nina phase is increasing these extremes for winter. This can be because the La Nina phase is stronger in the winter time [80]. Other EPIs show the same negative correlations for the SOI, but significant trends are exhibited for fewer stations. The ONI shows an opposite trend to the SOI for most of the stations, that is, significant positive correlations are exhibited for almost all of the EPIs, but the CDD index shows anomalous behavior as it also shows a positive trend with the ONI, resulting in an increase in the CDD index for El Nino conditions and a decrease in La Nina conditions, which can be further elaborated as drought conditions may prevail in El Nino conditions. The dry conditions prevailing and other precipitation indices not giving up to the mark result are because in the winter, rainfall is suppressed and is influenced by La Nina, as it was confirmed by [56]. The spatial variation of the ENSO for various regions can be due to other phenomena at play, like the monsoons, the westerlies, and the orographic variations. Such phenomena can affect the impact of the ENSO on the UIB. Similarly, global warming is also affecting the ENSO anomalies, as there is an extension towards the east of the warm front pool of the western Pacific [81]. The spatial patterns of the ENSO correlations with the EPIs are represented in Figures 16–19.
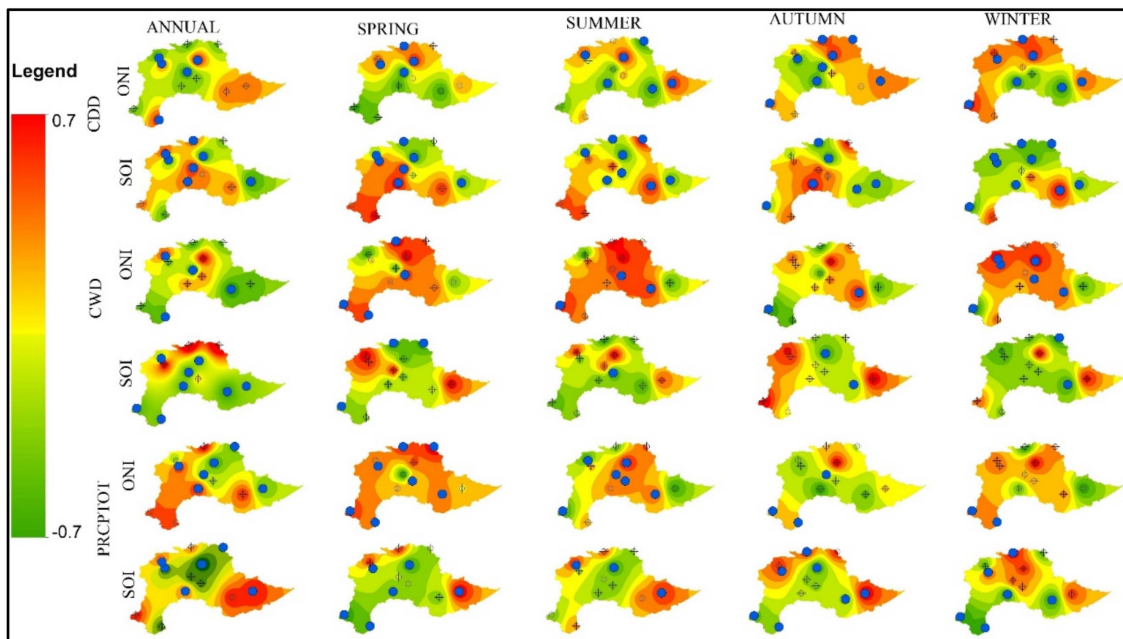
Figure 16. Spatial patterns of ENSO correlations with EPIs (PRCPTOT, CWD, CDD).
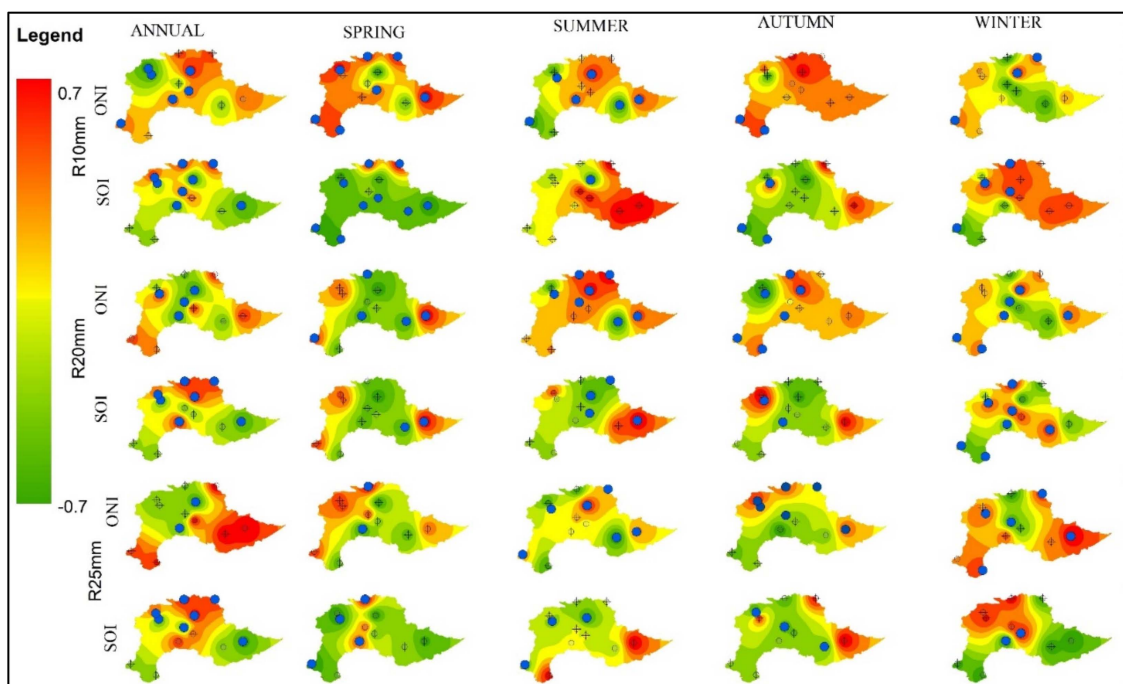
Figure 17. Spatial patterns of ENSO correlations with EPIs (R10 to R25).
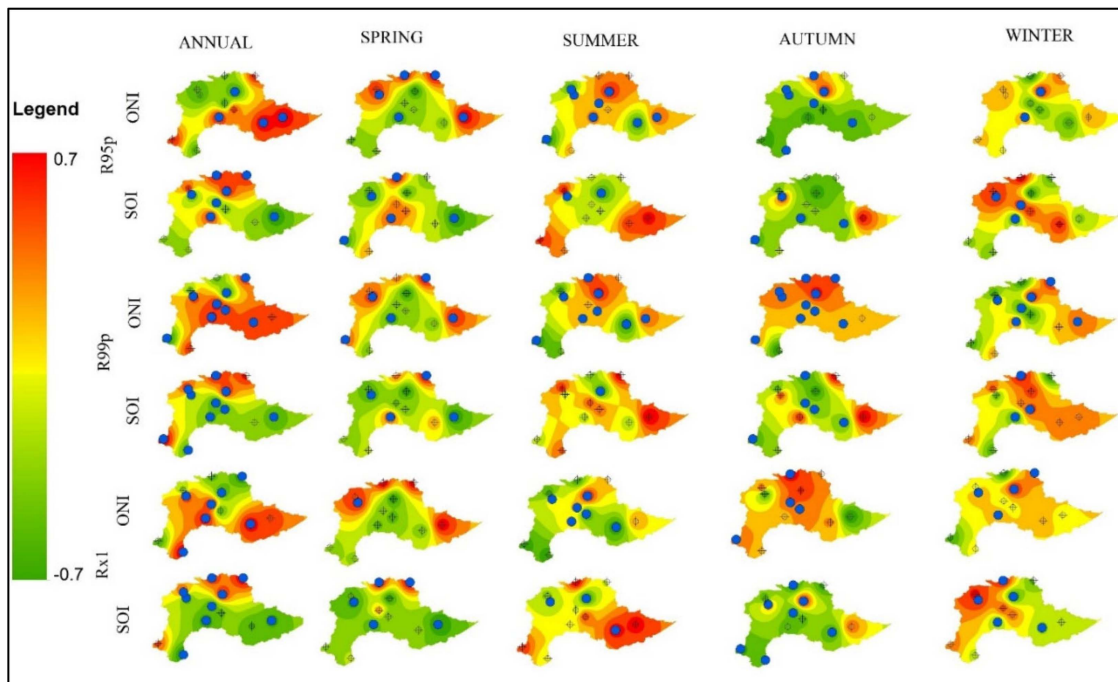
Figure 18. Spatial patterns of ENSO correlations with EPIs (Rx1, R99p and R95p).
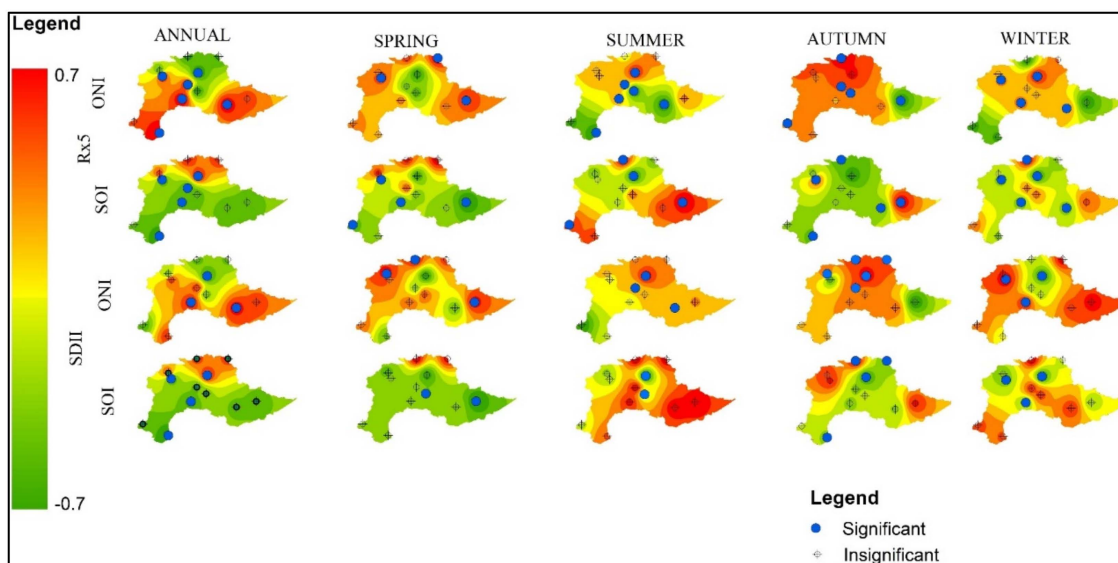
Figure 19. Spatial patterns of ENSO correlations with EPIs (SDII, Rx5).

3.8. Overall Trends in UIB

The impact of the ENSO was analyzed over the UIB in an annual time series. The three large-scale climate indices used include the SOI, ONI, and Nino 3.4 index, which were correlated with 11 extreme precipitation indices, giving an overall pattern of the ENSO's impact on the UIB. The results exhibited that the atmospheric index of the ENSO, i.e., the SOI, had a significant positive correlation with the CDD (36%) and CWD (37%) indices. The remaining nine indices had significant negative correlations with the SOI, emphasizing the fact that the El Nino phase of the SOI causes more extreme precipitation annually, whereas the La Nina phase of the SOI is followed by dry conditions. When investigating the correlation of the SST indices of the ENSO, i.e., the ONI and Nino 3.4, an opposite correlation was detected for the EPIs compared to the SOI. In the case of the ONI, all of the indices except for CWD exhibited significant negative correlations (36%)

with the ONI, whereas, on the other hand, Nino 3.4 had similar results as the ONI, with the CDD and CWD indices being negatively correlated, and the other 10 indices being positively correlated. The overall impact of the ENSO revealed that the atmospheric and sea surface temperature-related indices complement each other and form a coupled pattern in the climate, with a noteworthy impact on extreme events (Figure 20).
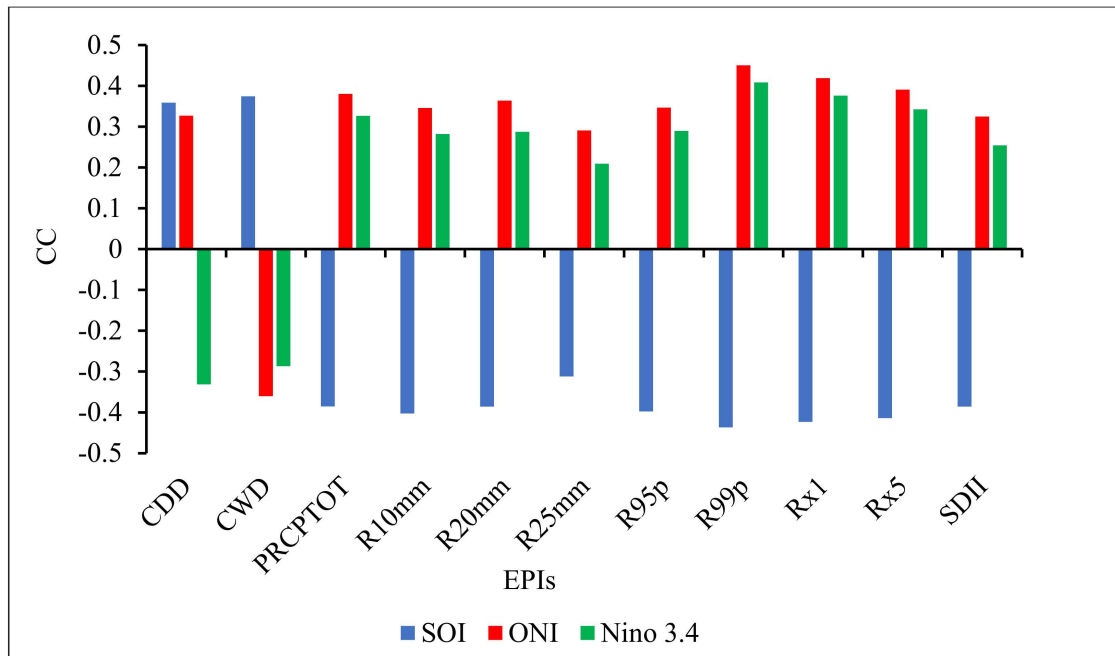
Figure 20. Overall correlation of ENSO with EPIs.

Highly Elevated Stations' Trends in UIB

It was observed that highly elevated stations, i.e., above a 3000 m elevation (Hushey, Khunjerab, Yasin, and Ziarat), exhibited different relationships with the ENSO indices. A further investigation revealed that for the SOI, all of the EPIs exhibited negative significant trends, except PRCPTOT, which depicted a positive insignificant trend. It was observed that PRCPTOT and CDD had opposite relationships with the SOI when observed during the overall study area correlation.

While investigating the trend of the ONI, it was observed that the correlations were not as significant as in the overall study area correlation. The CDD and Rx5 indices were the only two EPIs that had significant correlations with the ONI. It was also observed that the PRCPTOT and R25mm indices showed opposite results with the ONI when the correlation of the whole study area was analyzed.

Nino 3.4 gave insignificant results with the EPIs, except for R95p and R99p, and Rx5 had significant results with Nino 3.4. Further investigations revealed that CDD, PRCPTOT, and R25mm had opposite relationships compared to when it was observed for the whole study area (Figure 21).
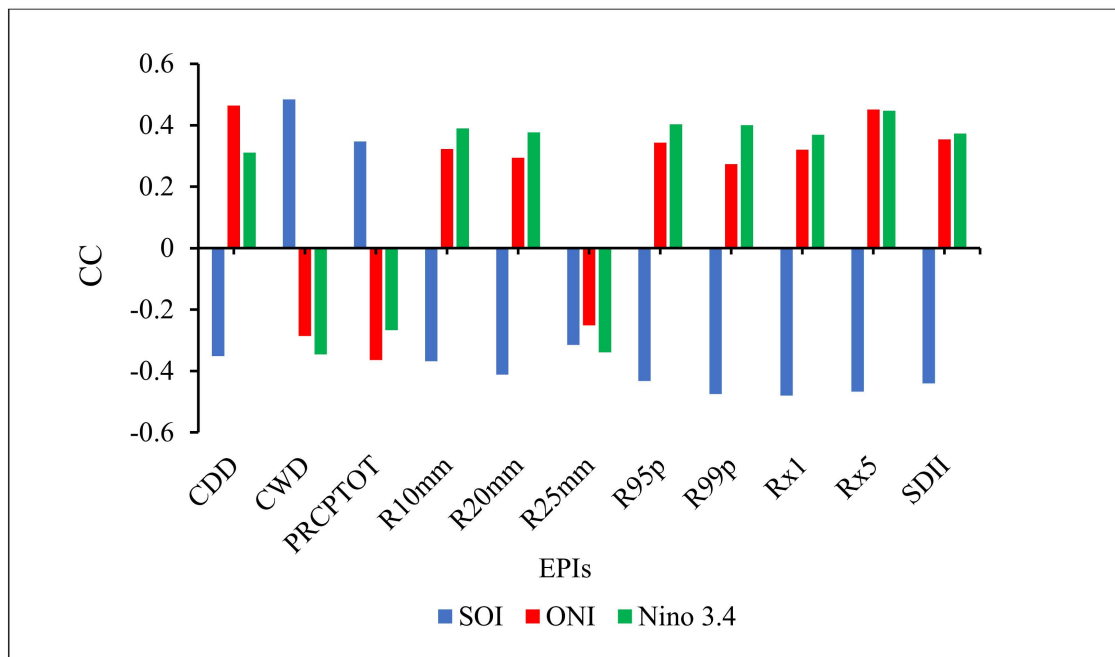
Figure 21. Highly elevated stations' correlations of ENSO with EPIs.

4. Conclusions

The purpose of this study was to analyze the effect of the ENSO on extreme rainfall in Pakistan. Based on a detailed analysis, the following conclusions are presented:

- An analysis of 132 time series revealed that 47% and 52% trends were significant for the MK test and ITA, respectively. CDD, CWD, and PRCPTOT showed mostly increasing significant trends for the EPIs.
- However, the CDD index is increasing by 0.13 days/year, whereas CWD is increasing by 0.09 days/year. This shows that the increase in CDD can cause drought conditions in the UIB.
- The very heavy precipitation days indices depicted decreasing trends for almost all of the regions and showed significant negative trends for two to four stations. However, it was seen that the overall magnitudes of R10 and R20mm were increasing with small rates of 0.06 and 0.02 days/year.
- Rx1 and Rx5 are decreasing at the rates of 0.08 and 0.05 mm/year, with eight stations showing decreasing trends, but only three to four stations showed significant trends.
- R95p and R99p also depicted decreasing trends for eight stations, but an overall increase in the magnitudes of 0.11 and 0.08 mm/days was observed.
- On the other hand, the SDII exhibited a decrease in magnitude by 0.02 mm/day/year. Nine stations displayed decreasing trends, with five stations showing significant trends.
- The climate indices revealed that there is a very slow increase in precipitation extremes for most of the indices, and decreasing trends in the Rx1, Rx5, and SDII indices.
- The correlation analysis revealed that the CDD index is significantly positively correlated with the ENSO indices during the winter period, and the inverse is true in the warm period. We can accept that the ENSO can reduce CDD in the warm phase and can increase CDD in the cold phase, as the warm phase, El Nino, increases precipitation.
- PRCPTOT exhibited a significant negative relationship with the SOI which indicates the increase in total precipitation during the El Nino phase of the ENSO.
- R95p and R99p also displayed negative relationships with the SOI in most of the stations, revealing that El Nino can cause more precipitation in the area.
- The maximum number of 1-day and 5-day precipitation indices also revealed that there is an increase in such days during the El Nino phase, causing more precipitation.

The ENSO is a global phenomenon that can have a significant effect on the climate of Pakistan. Therefore, it is recommended that the concerned departments should consider the impact of the ENSO while planning the water resources of the country. The ENSO impacts on temperature and elevation should also be measured to understand the ENSO better, as it can affect the climate of the country significantly.

Conflicts of Interest: The author Miklas Scholz is employed by aconium GmbH (previously atene KOM), Kunststoff-Technik Adams and Nexus by Sweden. The remaining authors declare that the research was conducted in the absence of any commercial or financial relationships that could be construed as a potential conflict of interest.

Appendix A
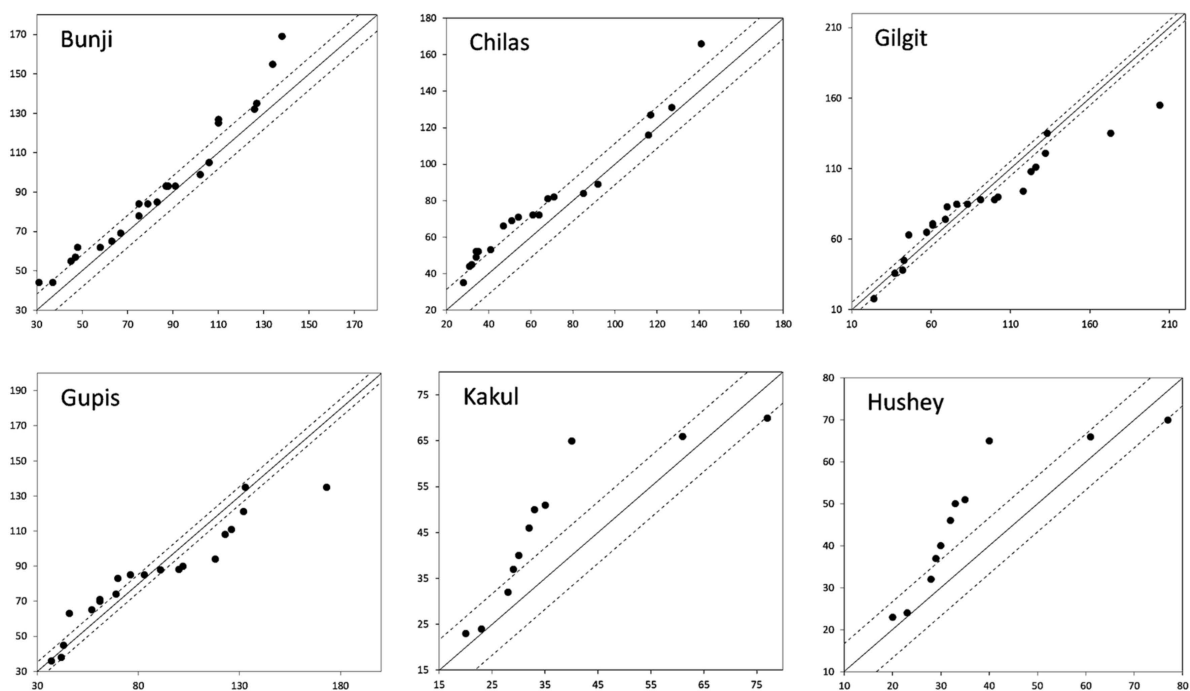
Figure A1. *Cont.*
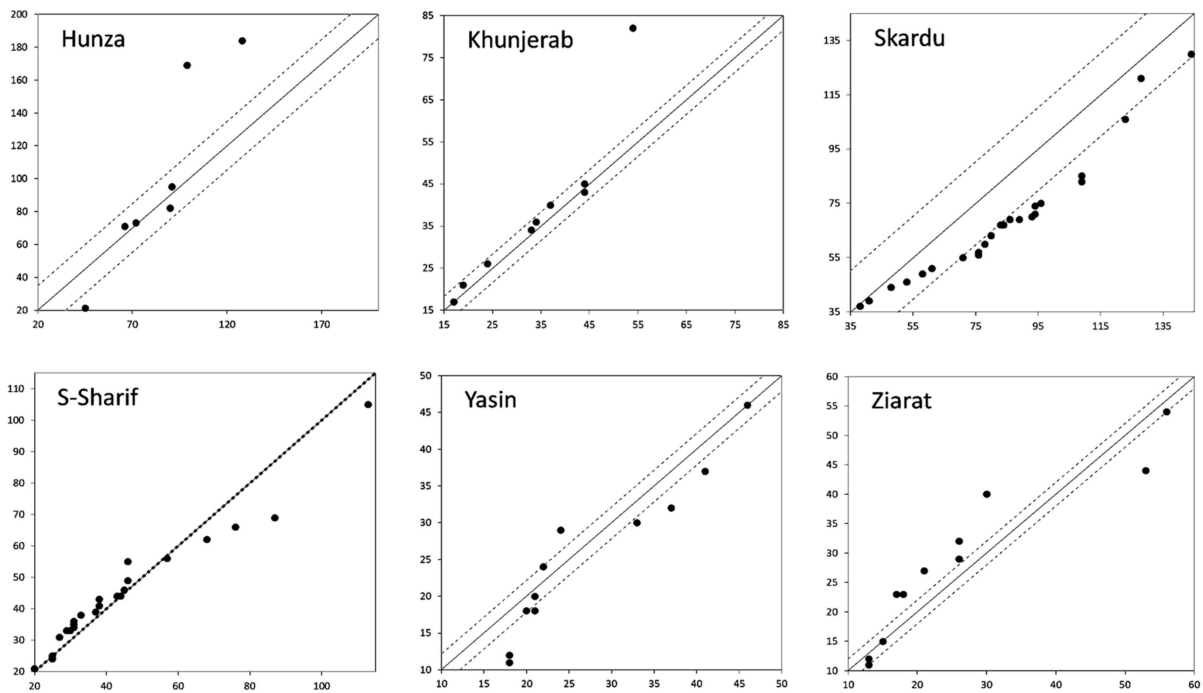
Figure A1. Results of CDD at 12 stations, obtained by using the ITA method.
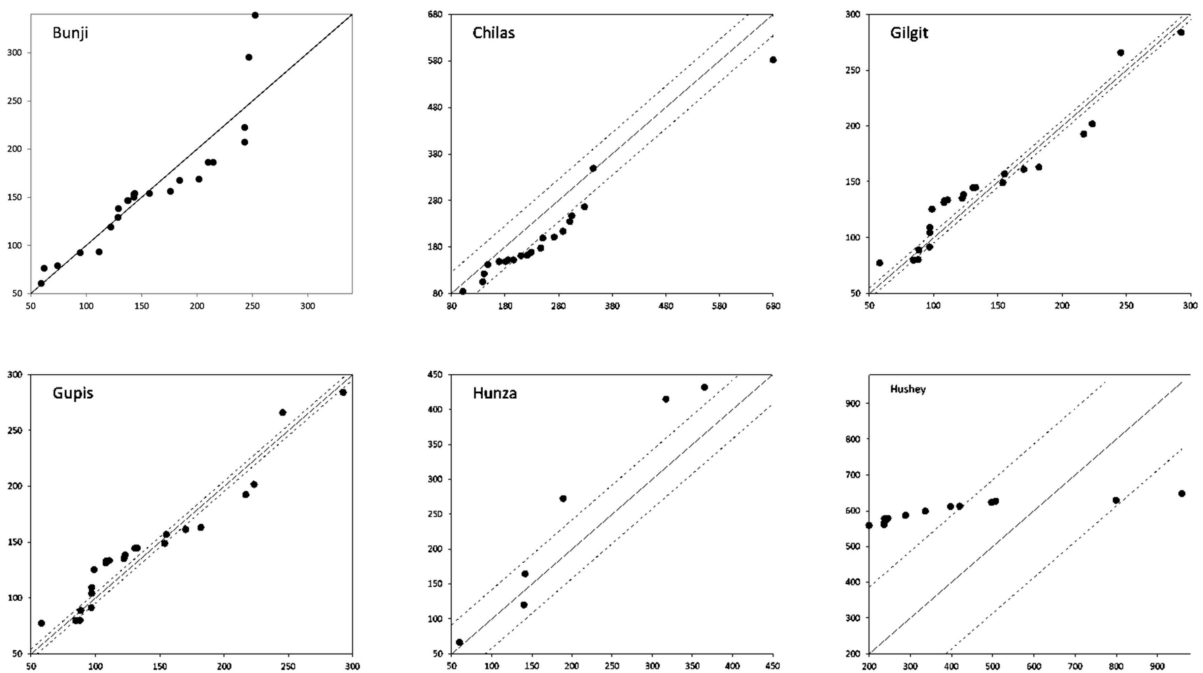
Figure A2. *Cont.*
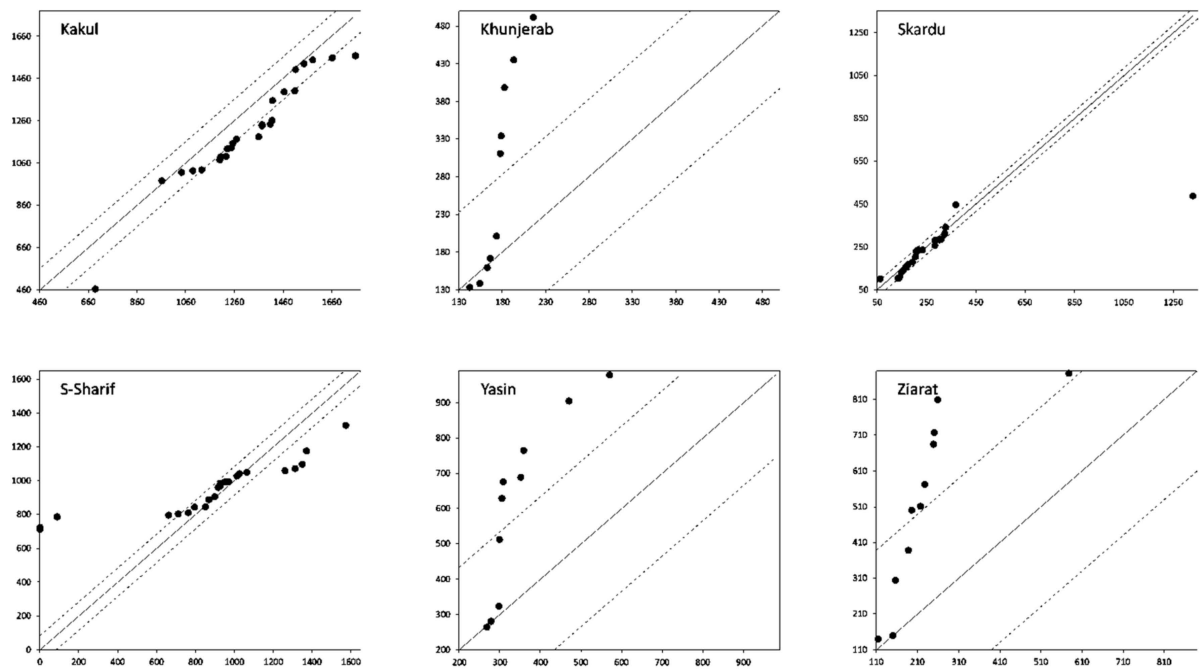
Figure A2. Results of PRCPTOT at 12 stations, obtained by using the ITA method.
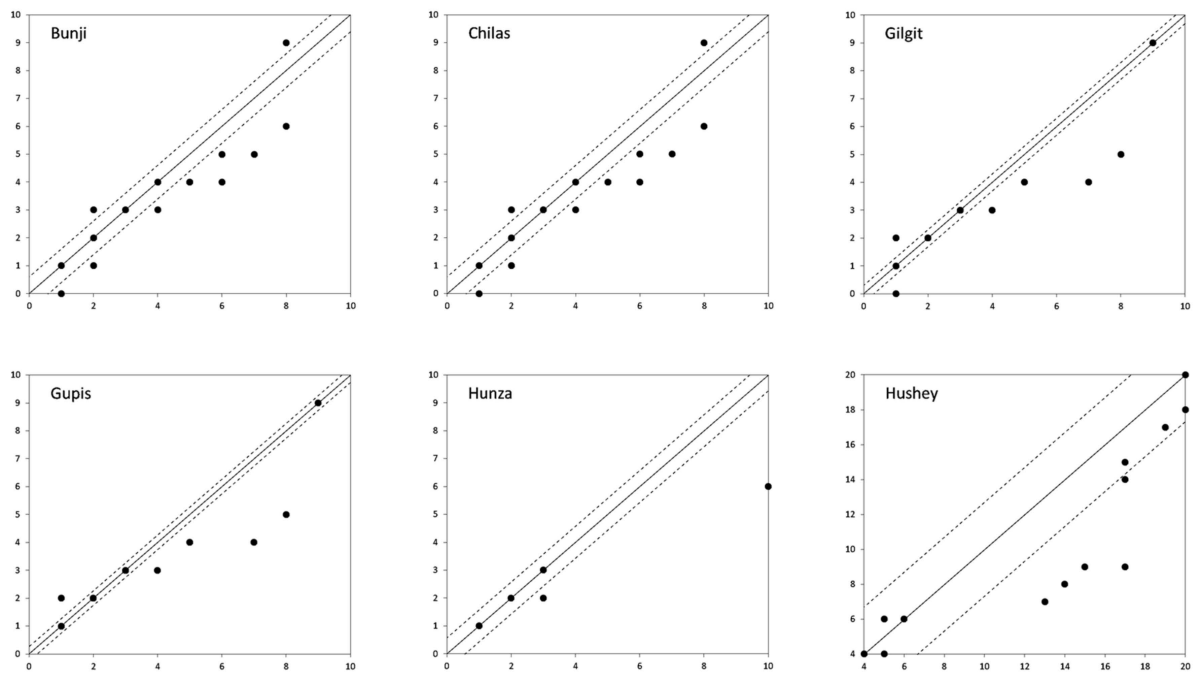
Figure A3. *Cont.*
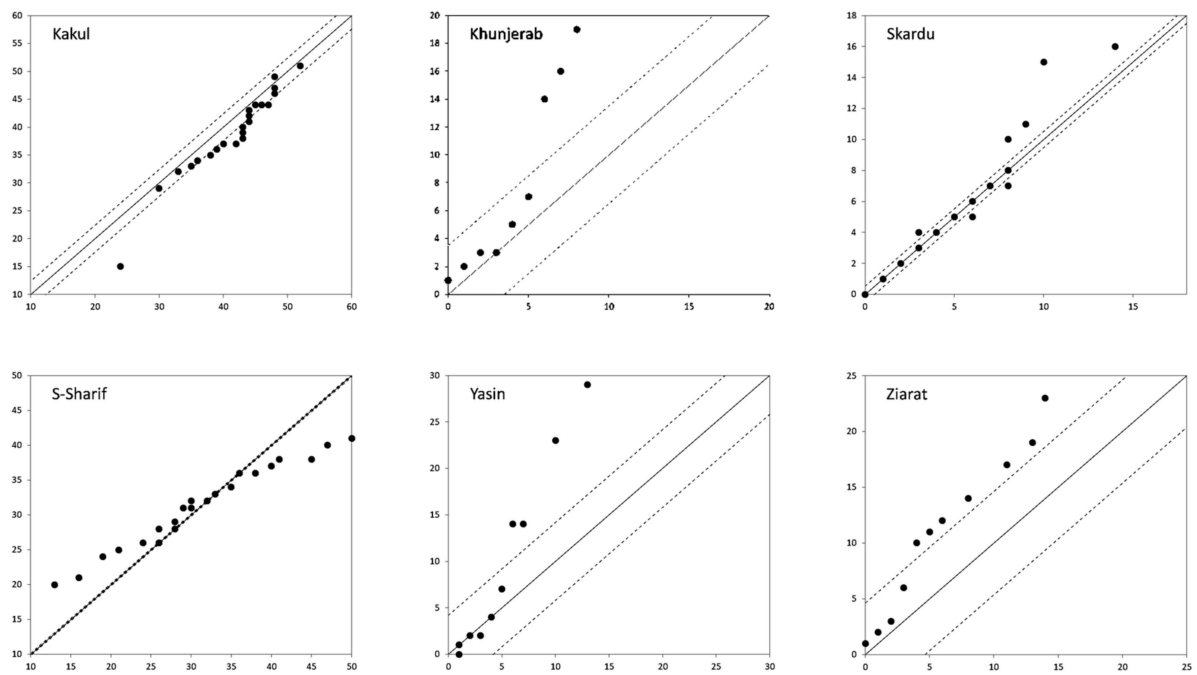
Figure A3. Results of R10mm at 12 stations, obtained by using the ITA method.
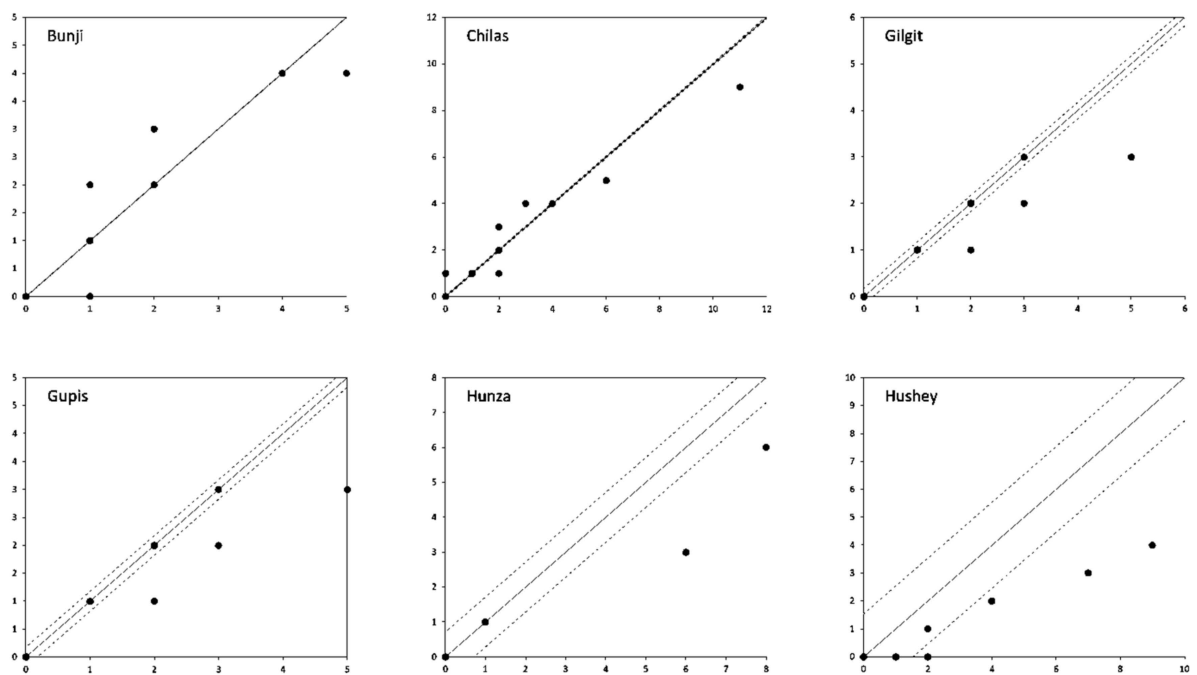
Figure A4. *Cont*.
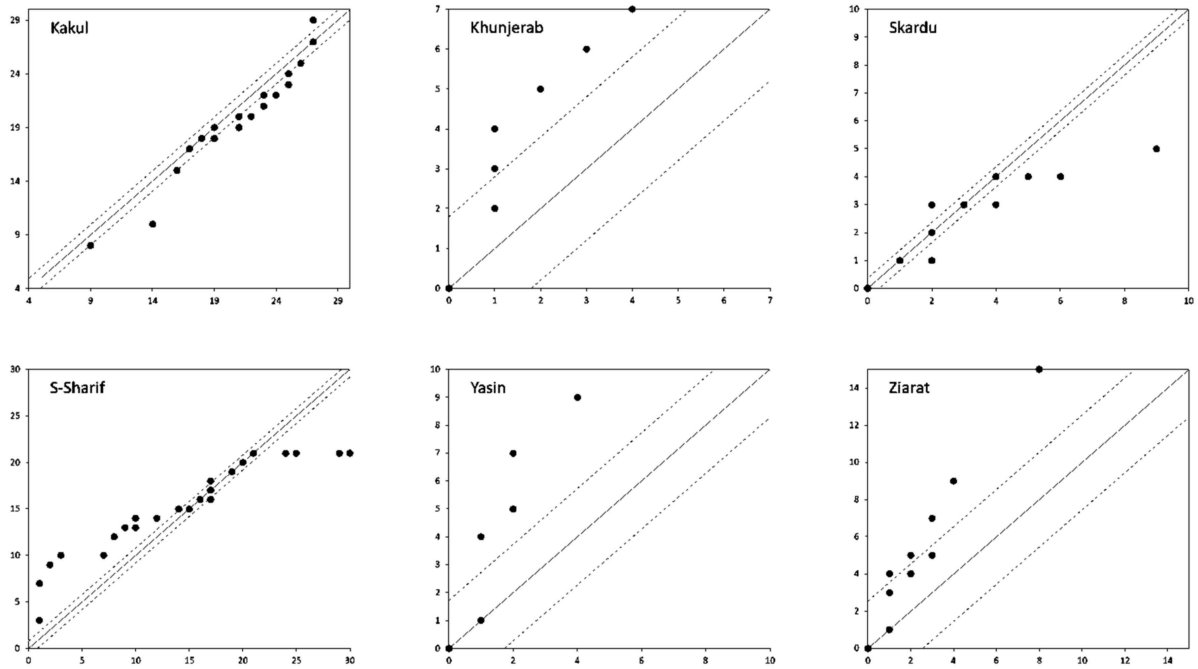
Figure A4. Results of R20mm at 12 stations, obtained by using the ITA method.
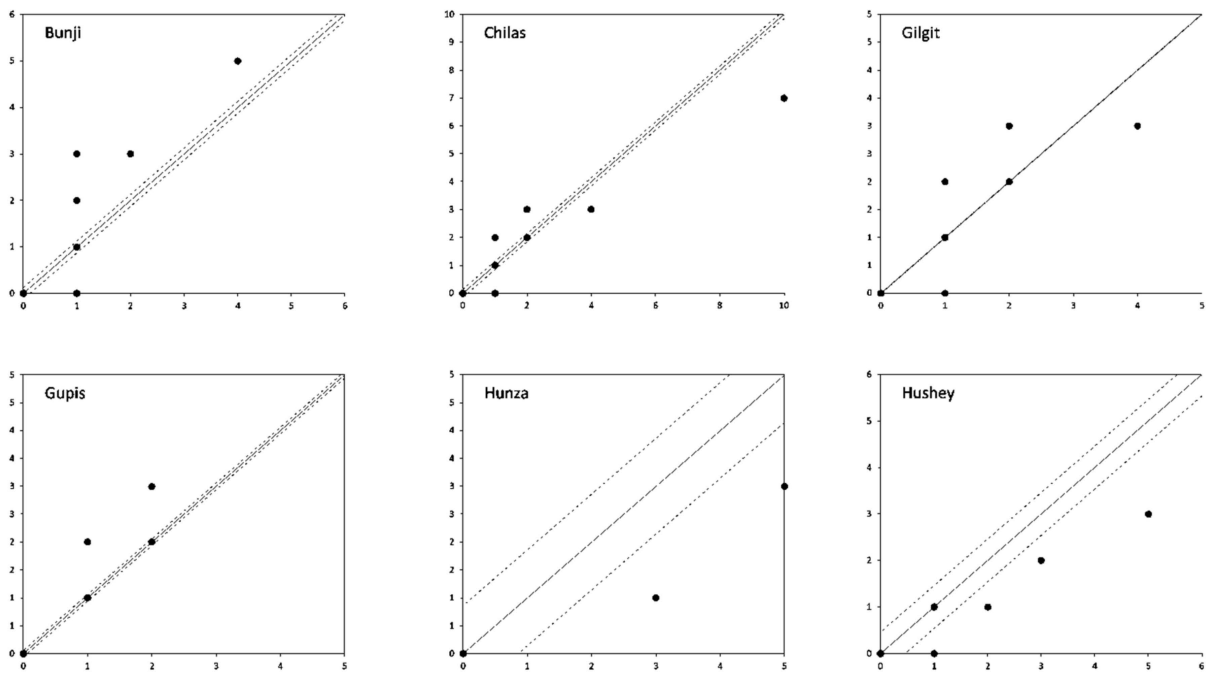
Figure A5. *Cont*.
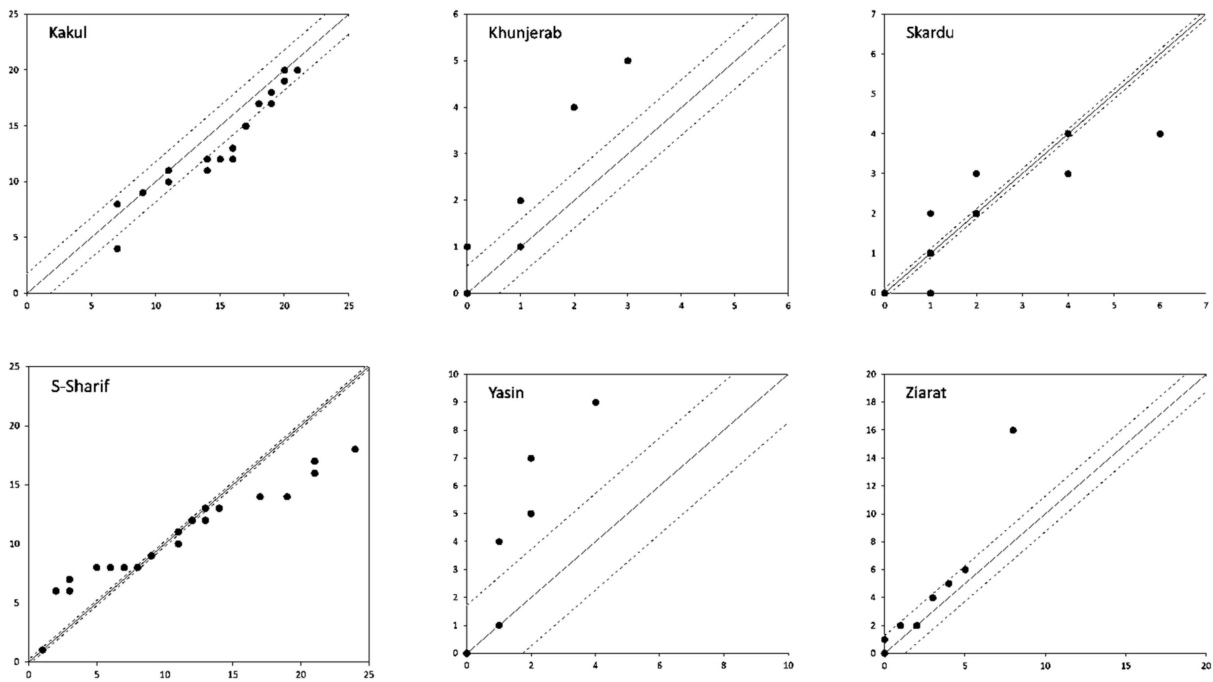
Figure A5. Results of R25mm at 12 stations, obtained by using the ITA method.
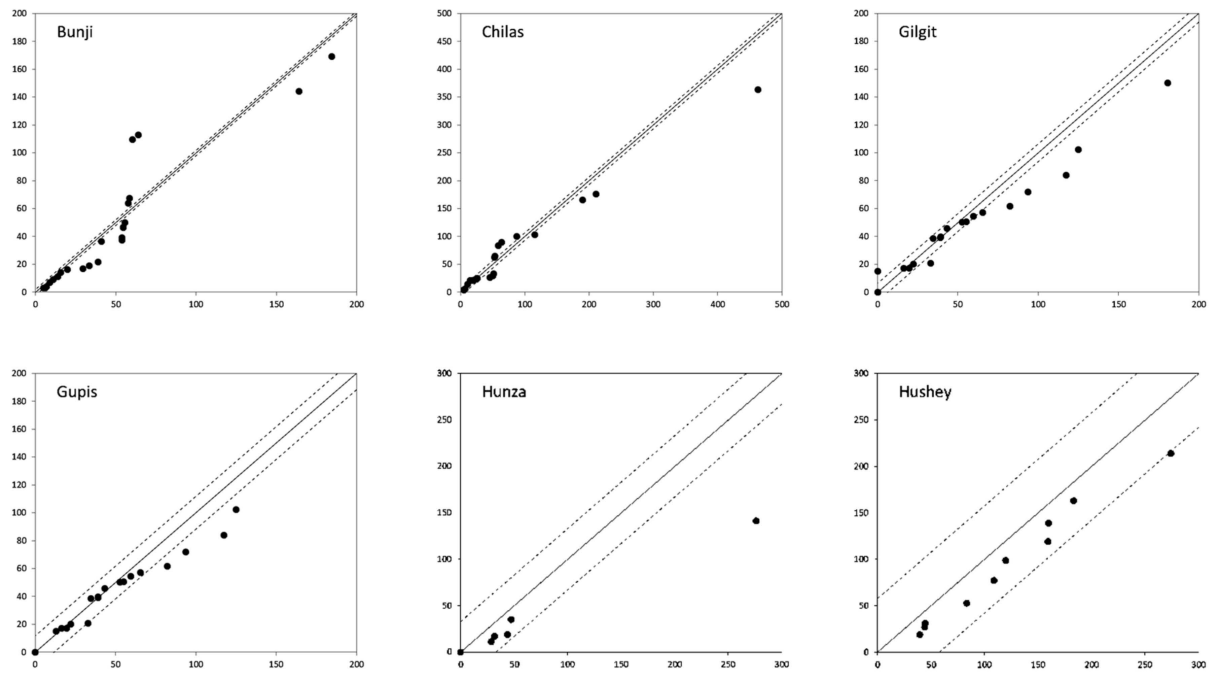
Figure A6. *Cont.*
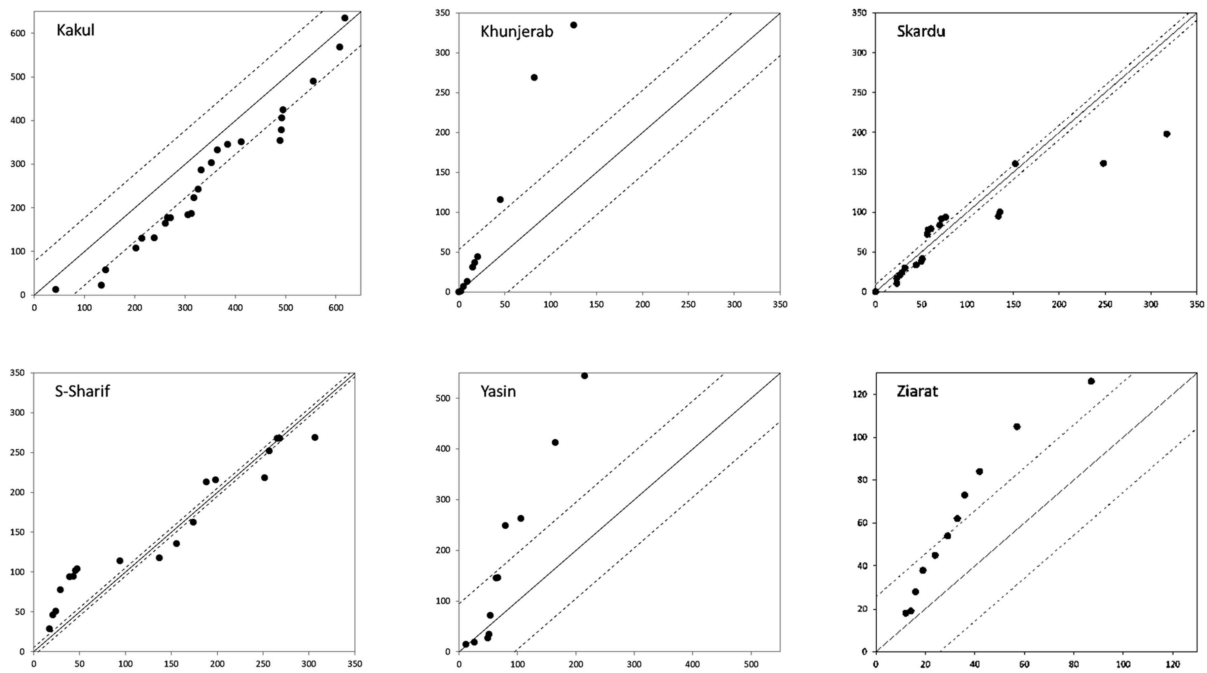
Figure A6. Results of R95p at 12 stations, obtained by using the ITA method.
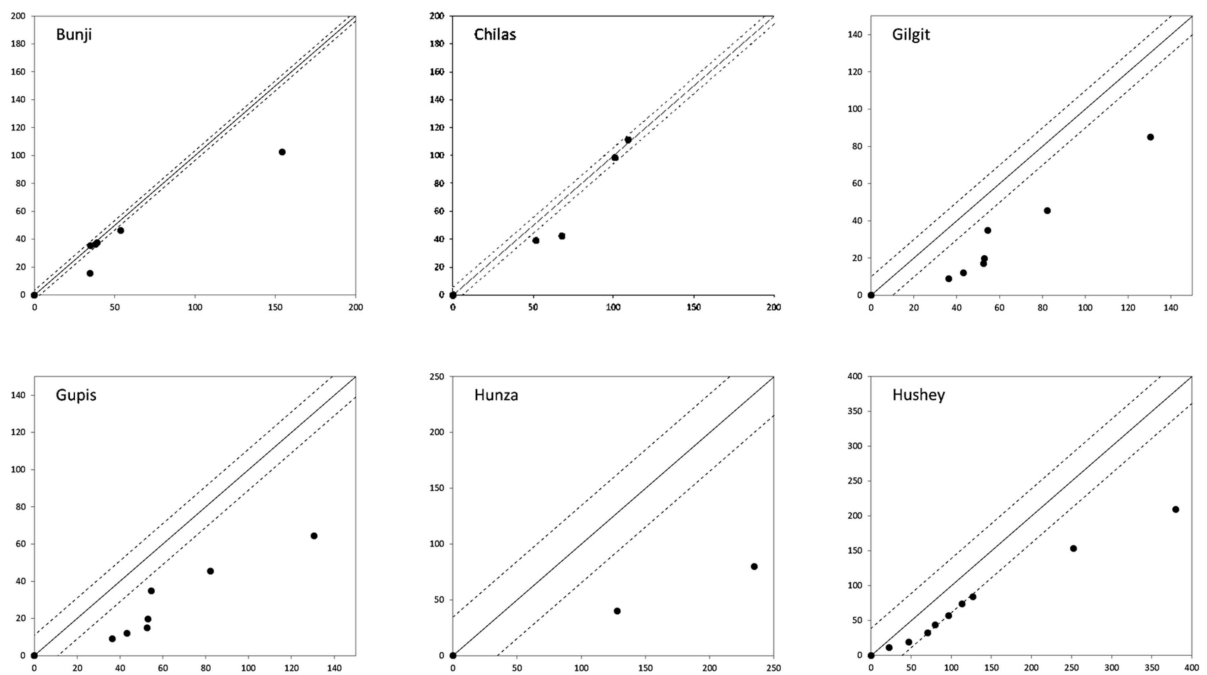
Figure A7. *Cont*.
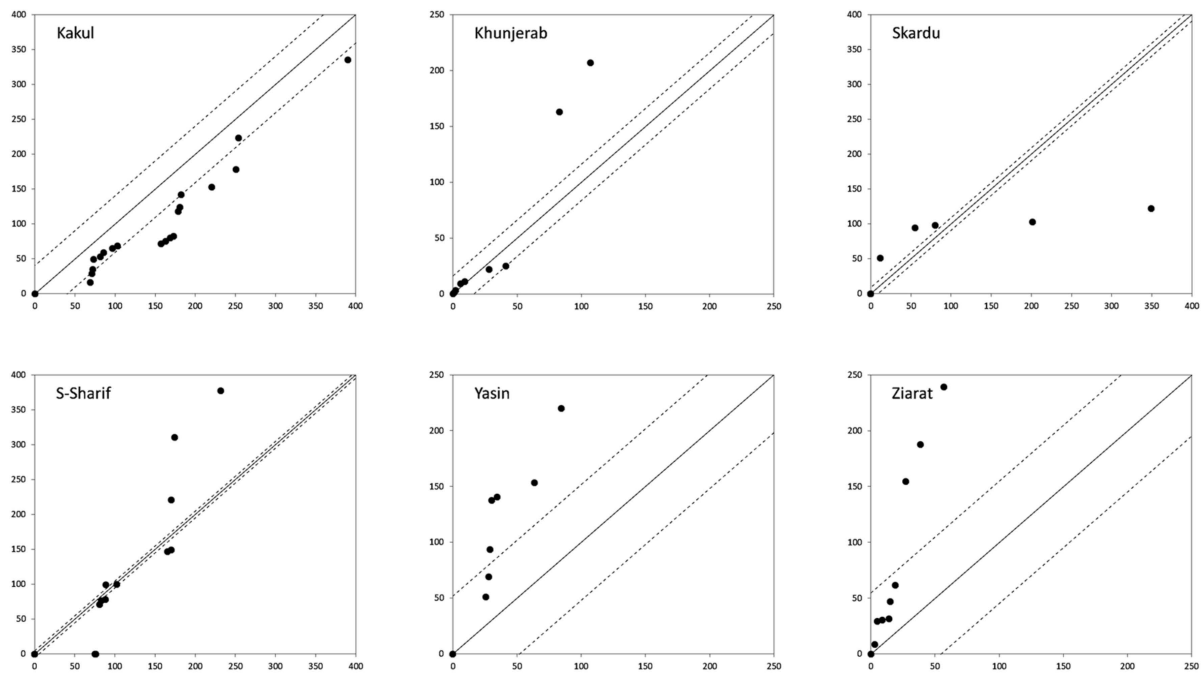
Figure A7. Results of R99p at 12 stations, obtained by using the ITA method.
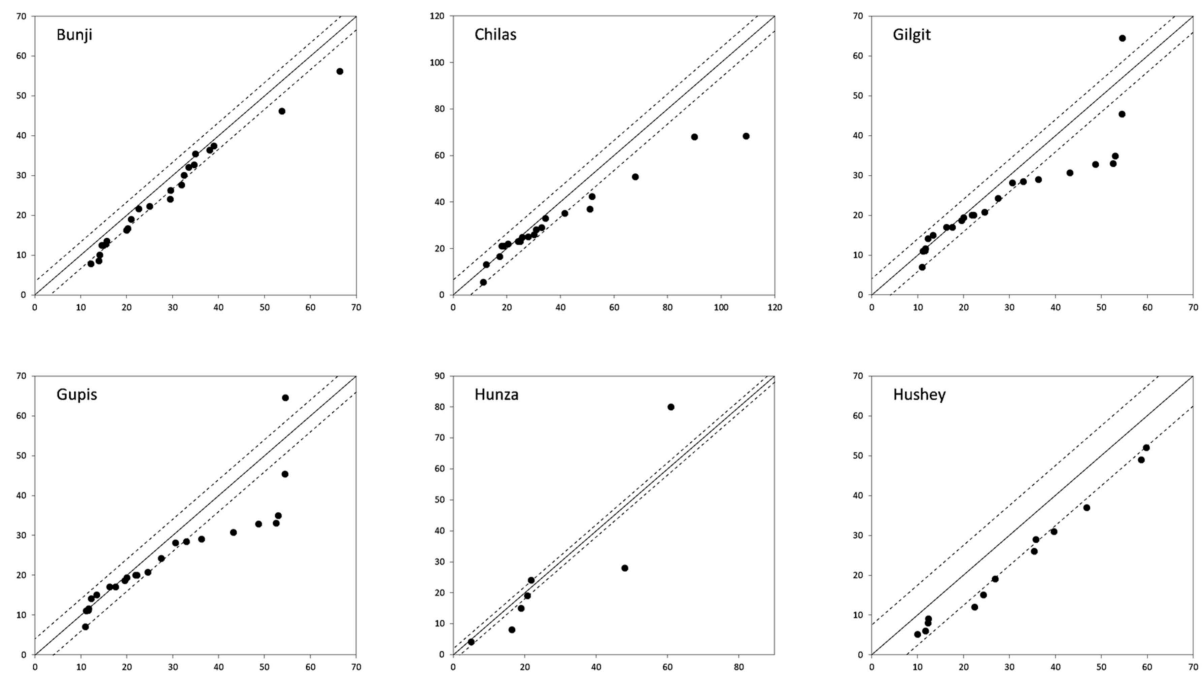
Figure A8. *Cont.*
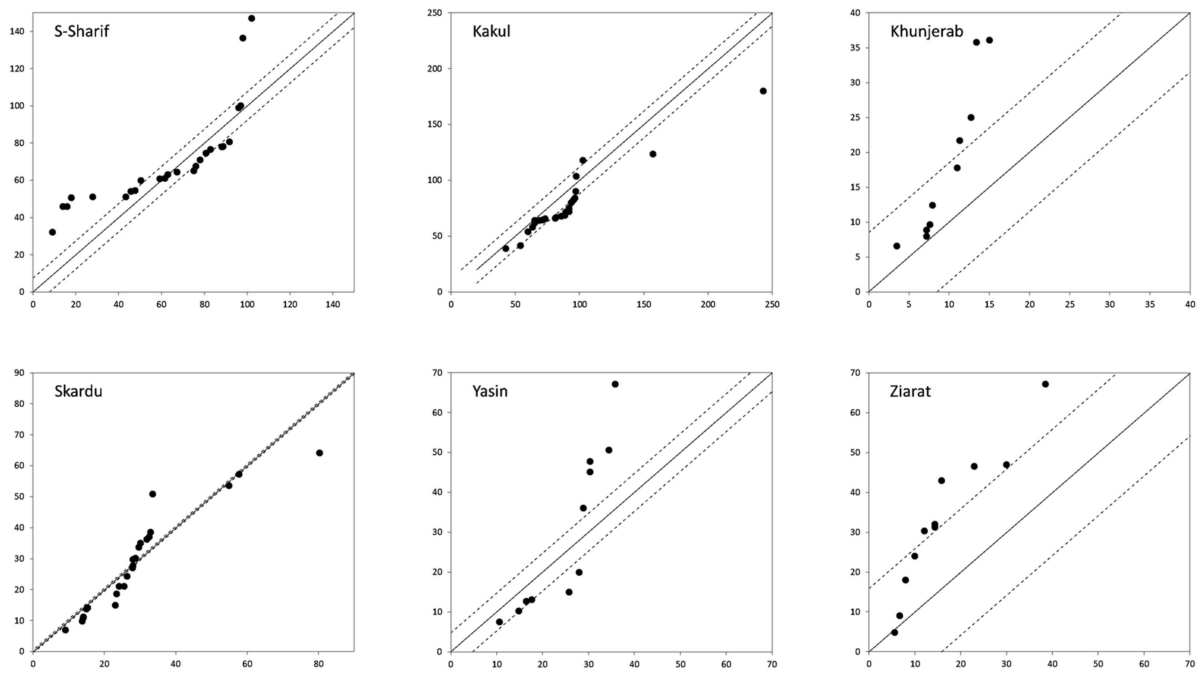
Figure A8. Results of Rx1 at 12 stations, obtained by using the ITA method.
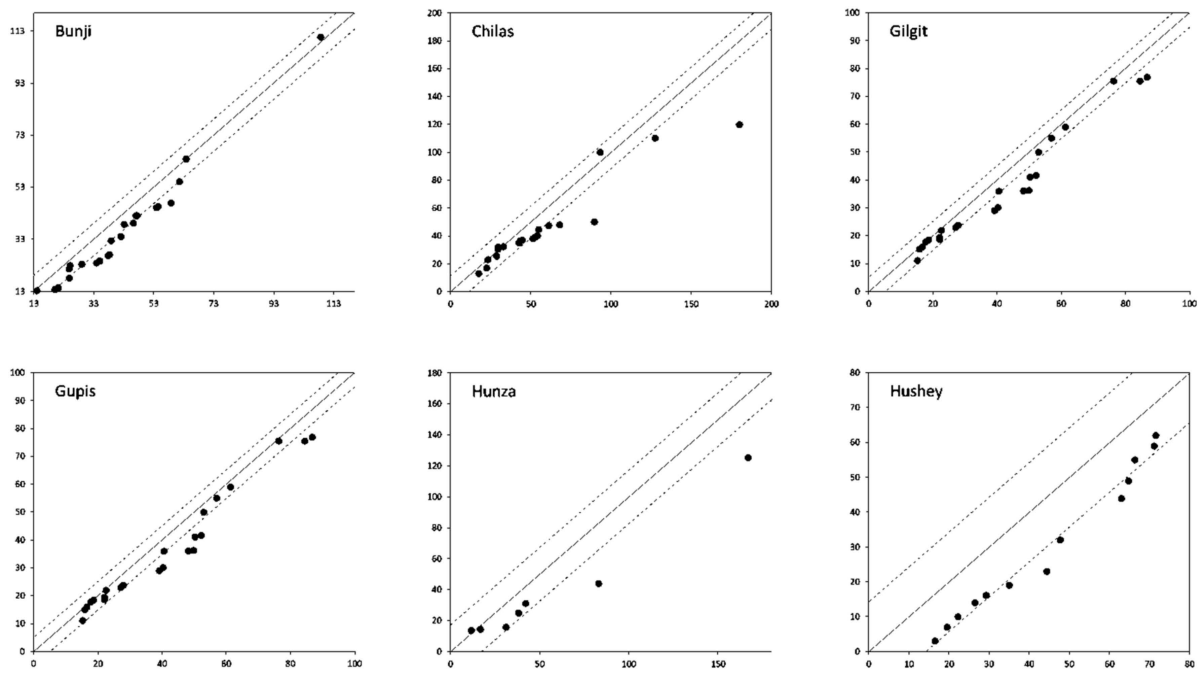
Figure A9. *Cont*.
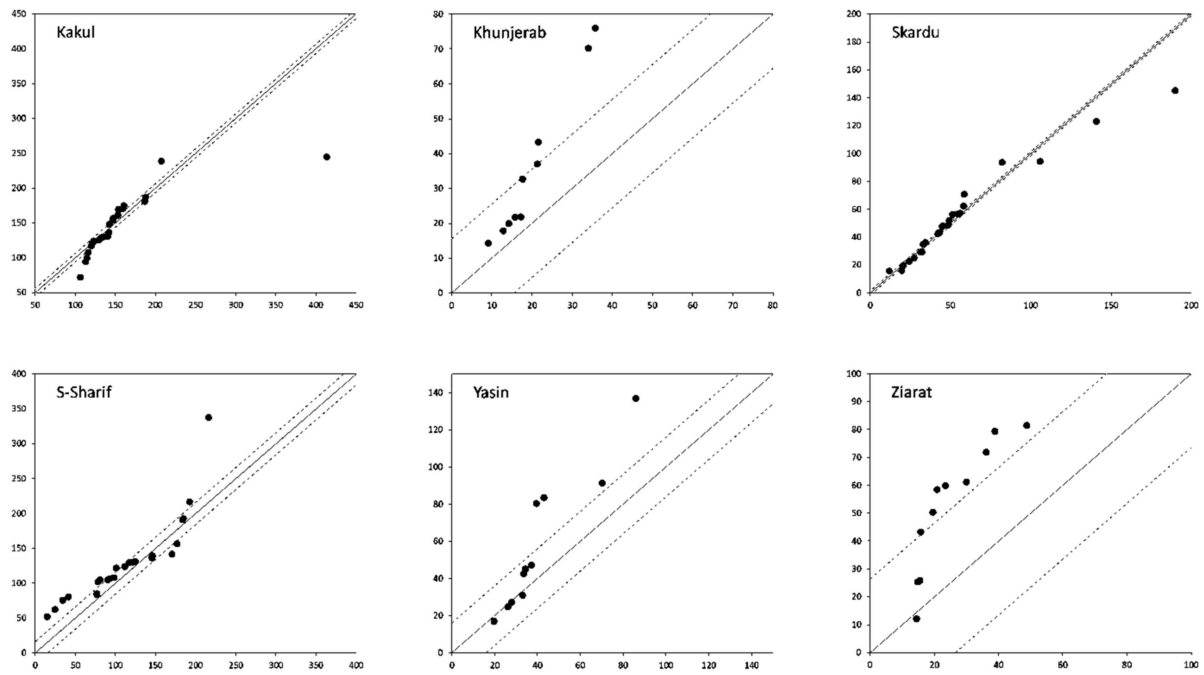
Figure A9. Results of Rx5 at 12 stations, obtained by using the ITA method.
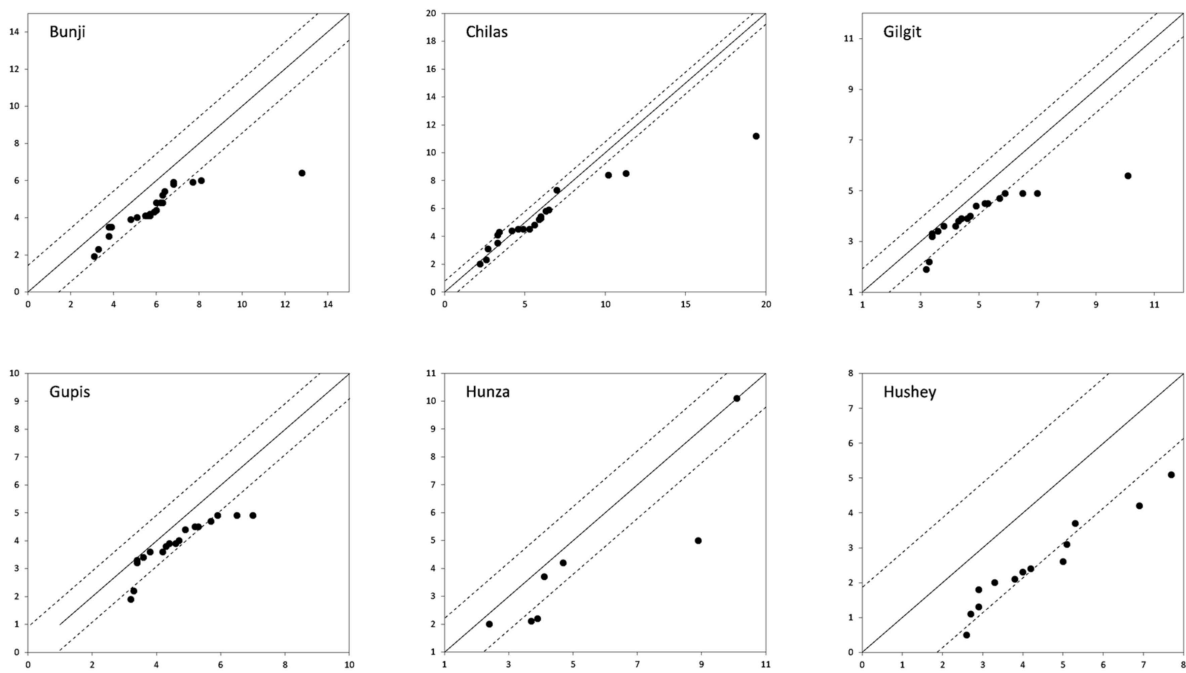
Figure A10. *Cont*.
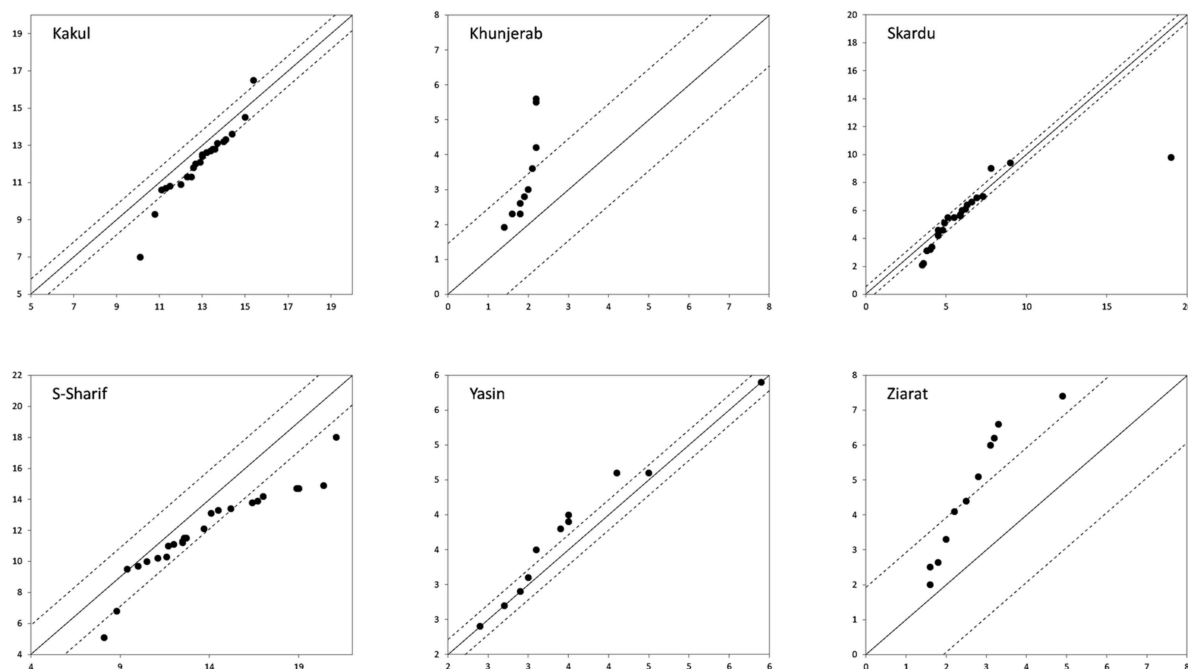
Figure A10. Results of SDII at 12 stations, obtained by using the ITA method.

References

1. Zhou, G.; Li, W.; Zhou, X.; Tan, Y.; Lin, G.; Li, X.; Deng, R. An innovative echo detection system with STM32 gated and PMT adjustable gain for airborne LiDAR. *Int. J. Remote Sens.* **2021**, *42*, 9187–9211. [CrossRef]
2. Zhou, G.; Deng, R.; Zhou, X.; Long, S.; Li, W.; Lin, G.; Li, X. Gaussian Inflection Point Selection for LiDAR Hidden Echo Signal Decomposition. *IEEE Geosci. Remote Sens. Lett.* **2021**, *19*, 6502705. [CrossRef]
3. Zhou, G.; Zhang, R.; Huang, S. Generalized Buffering Algorithm. *IEEE Access* **2021**, *9*, 27140–27157. [CrossRef]
4. Hashmi, H.N.; Siddiqui, Q.T.M.; Ghumman, A.R.; Kamal, M.A.; Mughal, H.U.R. A critical analysis of 2010 floods in Pakistan. *Afr. J. Agric. Res.* **2012**, *7*, 1054–1067. [CrossRef]
5. Gaurav, K.; Sinha, R.; Panda, P.K. The Indus flood of 2010 in Pakistan: A perspective analysis using remote sensing data. *Nat. Hazards* **2011**, *59*, 1815–1826. [CrossRef]
6. Carter, B.; Pozarny, P. *National Disaster Management Authorities*; GSDRC Helpdesk Research Report 1359; University of Birmingham: Birmingham, UK, 2016.
7. Khan, A.N.; Khan, S.N. Drought Risk and Reduction Approaches in Pakistan. In *Drought Risk and Reduction Approaches in Pakistan*; Springer: Berlin/Heidelberg, Germany, 2015; pp. 131–143.
8. Hirons, L.; Klingaman, N. La Niña 2016/2017: Historical Impact Analysis. 2016. Available online: https://www.gov.uk/research-for-development-outputs/la-nina-2016-2017-historical-impact-analysis (accessed on 12 December 2023).
9. Tian, H.F.; Huang, N.; Niu, Z.; Qin, Y.C.; Pei, J.; Wang, J. Mapping Winter Crops in China with Multi-Source Satellite Imagery and Phenology-Based Algorithm. *Remote Sens.* **2019**, *11*, 820. [CrossRef]
10. Tian, H.; Pei, J.; Huang, J.; Li, X.; Wang, J.; Zhou, B.; Qin, Y.; Wang, L. Garlic and Winter Wheat Identification Based on Active and Passive Satellite Imagery and the Google Earth Engine in Northern China. *Remote Sens.* **2020**, *12*, 3539. [CrossRef]
11. Yu, L.; Zhong, S.; Heilman, W.E.; Bian, X. A comparison of the effects of El Niño and El Niño Modoki on subdaily extreme precipitation occurrences across the contiguous United States. *J. Geophys. Res. Atmos.* **2017**, *122*, 7401–7415. [CrossRef]
12. Gao, C.; Hao, M.; Chen, J.; Gu, C. Simulation and design of joint distribution of rainfall and tide level in Wuchengxiyu Region, China. *Urban Clim.* **2021**, *40*, 101005. [CrossRef]
13. Xu, Z.; Li, X.; Li, J.; Xue, Y.; Jiang, S.; Liu, L.; Luo, Q.; Wu, K.; Zhang, N.; Feng, Y.; et al. Characteristics of Source Rocks and Genetic Origins of Natural Gas in Deep Formations, Gudian Depression, Songliao Basin, NE China. *ACS Earth Space Chem.* **2022**, *6*, 1750–1771. [CrossRef]
14. DeFlorio, M.J.; Pierce, D.W.; Cayan, D.R.; Miller, A.J. Western U.S. Extreme Precipitation Events and Their Relation to ENSO and PDO in CCSM4. *J. Clim.* **2013**, *26*, 4231–4243. [CrossRef]
15. Goly, A.; Teegavarapu, R.S.V. Individual and coupled influences of AMO and ENSO on regional precipitation characteristics and extremes. *Water Resour. Res.* **2014**, *50*, 4686–4709. [CrossRef]
16. Xu, J.; Lan, W.; Ren, C.; Zhou, X.; Wang, S.; Yuan, J. Modeling of coupled transfer of water, heat and solute in saline loess considering sodium sulfate crystallization. *Cold Reg. Sci. Technol.* **2021**, *189*, 103335. [CrossRef]
17. Rashid, A. Impact of el-nino on summer monsoon rainfall of pakistan. *Pak. J. Meteorol.* **2004**, *1*, 35–43.

18.   Mahmood, A.; Khan, T.M.A.; Faisal, N. Correlation between multivariate enso index (mei) and pakistan's summer rainfall. *Pak. J. Meteorol.* **2004**, *1*, 53–64.

19.   Hoyt, J.C. *Drought of 1936, with Discussion on the Significance of Drought in Relation to Climate*; U.S. Government Publishing Office: Washington, DC, USA, 1938. [CrossRef]

20.   Zhu, X.; Xu, Z.; Liu, Z.; Liu, M.; Yin, Z.; Yin, L.; Zheng, W. Impact of dam construction on precipitation: A regional perspective. *Mar. Freshw. Res.* **2022**, *74*, 877–890. [CrossRef]

21.   Kaskaoutis, D.; Houssos, E.; Solmon, F.; Legrand, M.; Rashki, A.; Dumka, U.; Francois, P.; Gautam, R.; Singh, R. Impact of atmospheric circulation types on southwest Asian dust and Indian summer monsoon rainfall. *Atmos. Res.* **2018**, *201*, 189–205. [CrossRef]

22.   Masood, M.U.; Haider, S.; Rashid, M.; Aldlemy, M.S.; Pande, C.B.; Đurin, B.; Homod, R.Z.; Alshehri, F.; Elkhrachy, I. Quantifying the Impacts of Climate and Land Cover Changes on the Hydrological Regime of a Complex Dam Catchment Area. *Sustainability* **2023**, *15*, 15223. [CrossRef]

23.   Haider, S.; Masood, M.U.; Rashid, M.; Alshehri, F.; Pande, C.B.; Katipoğlu, O.M.; Costache, R. Simulation of the Potential Impacts of Projected Climate and Land Use Change on Runoff under CMIP6 Scenarios. *Water* **2023**, *15*, 3421. [CrossRef]

24.   Xie, X.; Xie, B.; Cheng, J.; Chu, Q.; Dooling, T. A simple Monte Carlo method for estimating the chance of a cyclone impact. *Nat. Hazards* **2021**, *107*, 2573–2582. [CrossRef]

25.   Wu, X.; Guo, S.; Qian, S.; Wang, Z.; Lai, C.; Li, J.; Liu, P. Long-range precipitation forecast based on multipole and preceding fluctuations of sea surface temperature. *Int. J. Clim.* **2022**, *42*, 8024–8039. [CrossRef]

26.   Yin, L.; Wang, L.; Li, T.; Lu, S.; Yin, Z.; Liu, X.; Li, X.; Zheng, W. U-Net-STN: A Novel End-to-End Lake Boundary Prediction Model. *Land* **2023**, *12*, 1602. [CrossRef]

27.   Yin, L.; Wang, L.; Keim, B.D.; Konsoer, K.; Yin, Z.; Liu, M.; Zheng, W. Spatial and wavelet analysis of precipitation and river discharge during operation of the Three Gorges Dam, China. *Ecol. Indic.* **2023**, *154*, 110837. [CrossRef]

28.   Gong, S.; Bai, X.; Luo, G.; Li, C.; Wu, L.; Chen, F.; Ran, C.; Xi, H.; Zhang, S. Climate change has enhanced the positive contribution of rock weathering to the major ions in riverine transport. *Glob. Planet. Chang.* **2023**, *228*, 104203. [CrossRef]

29.   Hussain, D.; Kuo, C.-Y.; Hameed, A.; Tseng, K.-H.; Jan, B.; Abbas, N.; Kao, H.-C.; Lan, W.-H.; Imani, M. Spaceborne Satellite for Snow Cover and Hydrological Characteristic of the Gilgit River Basin, Hindukush–Karakoram Mountains, Pakistan. *Sensors* **2019**, *19*, 531. [CrossRef] [PubMed]

30.   Hasson, S.U.; Böhner, J.; Lucarini, V. Prevailing climatic trends and runoff response from Hindukush–Karakoram–Himalaya, upper Indus Basin. *Earth Syst. Dyn.* **2017**, *8*, 337–355. [CrossRef]

31.   Anjum, M.N.; Ding, Y.; Shangguan, D. Simulation of the projected climate change impacts on the river flow regimes under CMIP5 RCP scenarios in the westerlies dominated belt, northern Pakistan. *Atmos. Res.* **2019**, *227*, 233–248. [CrossRef]

32.   Rashid, M.; Haider, S.; Masood, M.U.; Pande, C.B.; Tolche, A.D.; Alshehri, F.; Costache, R.; Elkhrachy, I. Sustainable Water Management for Small Farmers with Center-Pivot Irrigation: A Hydraulic and Structural Design Perspective. *Sustainability* **2023**, *15*, 16390. [CrossRef]

33.   Forsythe, N.; Fowler, H.J.; Blenkinsop, S.; Burton, A.; Kilsby, C.G.; Archer, D.R.; Harpham, C.; Hashmi, M.Z. Application of a stochastic weather generator to assess climate change impacts in a semi-arid climate: The Upper Indus Basin. *J. Hydrol.* **2014**, *517*, 1019–1034. [CrossRef]

34.   Bin Farhan, S.; Zhang, Y.; Aziz, A.; Gao, H.; Ma, Y.; Kazmi, J.; Shahzad, A.; Hussain, I.; Mansha, M.; Umar, M.; et al. Assessing the Impacts of Climate Change on the High Altitude Snow- and Glacier-Fed Hydrological Regimes of Astore and Hunza, the Sub-Catchments of Upper Indus Basin. *J. Water Clim. Chang.* **2018**, *11*, 479–490. [CrossRef]

35.   Nagra, M.; Masood, M.U.; Haider, S.; Rashid, M. Assessment of Spatiotemporal Droughts through Machine Learning Algorithm over Pakistan. In Proceedings of the 2nd National Conference on Sustainable Water Resources Management (SWRM-22) at Center of Excellence in Water Resources Engineering, UET, Lahore, Pakistan, 16 November 2022; p. 8670.

36.   Liu, Z.; Xu, J.; Liu, M.; Yin, Z.; Liu, X.; Yin, L.; Zheng, W. Remote sensing and geostatistics in urban water-resource monitoring: A review. *Mar. Freshw. Res.* **2023**, *74*, 747–765. [CrossRef]

37.   Zhang, S.; Bai, X.; Zhao, C.; Tan, Q.; Luo, G.; Wang, J.; Li, Q.; Wu, L.; Chen, F.; Li, C.; et al. Global CO_2 Consumption by Silicate Rock Chemical Weathering: Its Past and Future. *Earth's Future* **2021**, *9*, e1938E–e2020E. [CrossRef]

38.   Zhou, J.; Wang, L.; Zhong, X.; Yao, T.; Qi, J.; Wang, Y.; Xue, Y. Quantifying the major drivers for the expanding lakes in the interior Tibetan Plateau. *Sci. Bull.* **2021**, *67*, 474–478. [CrossRef] [PubMed]

39.   Khattak, M.S.; Babel, M.S.; Sharif, M. Hydro-meteorological trends in the upper Indus River basin in Pakistan. *Clim. Res.* **2011**, *46*, 103–119. [CrossRef]

40.   Archer, D.; Fowler, H. Spatial and temporal variations in precipitation in the Upper Indus Basin, global teleconnections and hydrological implications. *Hydrol. Earth Syst. Sci.* **2004**, *8*, 47–61. [CrossRef]

41.   Ullah, S.; You, Q.; Ullah, W.; Ali, A. Observed changes in precipitation in China-Pakistan economic corridor during 1980–2016. *Atmos. Res.* **2018**, *210*, 1–14. [CrossRef]

42.   Steinbauer, M.; Zeidler, J. Climate Change in the Northern Areas Pakistan: Impacts on Glaciers, Ecology and Livelyhoods. 2008. Available online: http://www.alfalter.org/wwfpakistan/Climate-change-in-the-Northern-Areas-Pakistan.pdf (accessed on 12 December 2023).

43. Latif, Y.; Yaoming, M.; Yaseen, M. Spatial analysis of precipitation time series over the Upper Indus Basin. *Theor. Appl. Clim.* **2016**, *131*, 761–775. [CrossRef]

44. Yin, L.; Wang, L.; Li, T.; Lu, S.; Tian, J.; Yin, Z.; Li, X.; Zheng, W. U-Net-LSTM: Time Series-Enhanced Lake Boundary Prediction Model. *Land* **2023**, *12*, 1859. [CrossRef]

45. Lin, X.; Zhu, G.; Qiu, D.; Ye, L.; Liu, Y.; Chen, L.; Liu, J.; Lu, S.; Wang, L.; Zhao, K.; et al. Stable precipitation isotope records of cold wave events in Eurasia. *Atmos. Res.* **2023**, *296*, 107070. [CrossRef]

46. Luo, J.; Niu, F.; Lin, Z.; Liu, M.; Yin, G.; Gao, Z. Abrupt increase in thermokarst lakes on the central Tibetan Plateau over the last 50 years. *CATENA* **2022**, *217*, 106497. [CrossRef]

47. Lüdecke, H.-J.; Müller-Plath, G.; Wallace, M.G.; Lüning, S. Decadal and multidecadal natural variability of African rainfall. *J. Hydrol. Reg. Stud.* **2021**, *34*, 100795. [CrossRef]

48. Shi, P.; Yang, T.; Xu, C.-Y.; Yong, B.; Shao, Q.; Li, Z.; Wang, X.; Zhou, X.; Li, S. How do the multiple large-scale climate oscillations trigger extreme precipitation? *Glob. Planet. Chang.* **2017**, *157*, 48–58. [CrossRef]

49. Fowler, H.J.; Archer, D.R. Hydro-Climatological Variability in the Upper Indus Basin and Implications for Water Resources. *IAHS-AISH Publ.* **2005**, *295*, 131–138.

50. Bhutiyani, M.R.; Kale, V.S.; Pawar, N.J. Climate change and the precipitation variations in the northwestern Himalaya: 1866–2006. *Int. J. Clim.* **2009**, *30*, 535–548. [CrossRef]

51. Wu, X.; Feng, X.; Wang, Z.; Chen, Y.; Deng, Z. Multi-source precipitation products assessment on drought monitoring across global major river basins. *Atmos. Res.* **2023**, *295*, 106982. [CrossRef]

52. Xiong, L.; Bai, X.; Zhao, C.; Li, Y.; Tan, Q.; Luo, G.; Wu, L.; Chen, F.; Li, C.; Ran, C.; et al. High-Resolution Data Sets for Global Carbonate and Silicate Rock Weathering Carbon Sinks and Their Change Trends. *Earth's Future* **2022**, *10*, e2022EF002746. [CrossRef]

53. Ma, S.; Qiu, H.; Yang, D.; Wang, J.; Zhu, Y.; Tang, B.; Sun, K.; Cao, M. Surface multi-hazard effect of underground coal mining. *Landslides* **2022**, *20*, 39–52. [CrossRef]

54. Basharat, M. Water Management in the Indus Basin in Pakistan: Challenges and Opportunities. *Indus River Basin* **2019**, *1*, 375–388.

55. Li, Q.; Lu, L.; Zhao, Q.; Hu, S. Impact of Inorganic Solutes' Release in Groundwater during Oil Shale In Situ Exploitation. *Water* **2022**, *15*, 172. [CrossRef]

56. Anwar, Z. El Nino and La Nina: Effects on Region and Pakistan; Islamabad. 2021. Available online: https://casstt.com/el-nino-and-la-nina-effects-on-region-and-pakistan (accessed on 12 December 2023).

57. Laghari, A.N.; Vanham, D.; Rauch, W. The Indus basin in the framework of current and future water resources management. *Hydrol. Earth Syst. Sci.* **2012**, *16*, 1063–1083. [CrossRef]

58. Shrestha, A.B.; Bajracharya, S.R.; Sharma, A.R.; Duo, C.; Kulkarni, A. Observed trends and changes in daily temperature and precipitation extremes over the Koshi river basin 1975–2010. *Int. J. Clim.* **2016**, *37*, 1066–1083. [CrossRef]

59. Zaman, M.; Ahmad, I.; Usman, M.; Saifullah, M.; Anjum, M.N.; Khan, M.I.; Qamar, M.U. Event-Based Time Distribution Patterns, Return Levels, and Their Trends of Extreme Precipitation across Indus Basin. *Water* **2020**, *12*, 3373. [CrossRef]

60. Lutz, A.F.; Immerzeel, W.W.; Kraaijenbrink, P.D.A.; Shrestha, A.B.; Bierkens, M.F.P. Climate Change Impacts on the Upper Indus Hydrology: Sources, Shifts and Extremes. *PLoS ONE* **2016**, *11*, e0165630. [CrossRef] [PubMed]

61. Karl, T.R.; Nicholls, N.; Ghazi, A. Clivar/GCOS/WMO Workshop on Indices and Indicators for Climate Extremes Workshop Summary. In *Weather and Climate Extremes: Changes, Variations and a Perspective from the Insurance Industry*; Springer: Berlin/Heidelberg, Germany, 1999; pp. 3–7.

62. Guo, J.; Guo, S.; Li, Y.; Chen, H.; Li, T. Spatial and temporal variation of extreme precipitation indices in the Yangtze River basin, China. *Stoch. Environ. Res. Risk Assess.* **2012**, *27*, 459–475. [CrossRef]

63. Mann, H.B. Nonparametric tests against trend. *Econometrica* **1945**, *13*, 245–259. [CrossRef]

64. Tabari, H.; Marofi, S.; Aeini, A.; Talaee, P.H.; Mohammadi, K. Trend analysis of reference evapotranspiration in the western half of Iran. *Agric. For. Meteorol.* **2011**, *151*, 128–136. [CrossRef]

65. Şen, Z. Innovative Trend Analysis Methodology. *J. Hydrol. Eng.* **2012**, *17*, 1042–1046. [CrossRef]

66. Pastagia, J.; Mehta, D. Application of innovative trend analysis on rainfall time series over Rajsamand district of Rajasthan state. *Water Supply* **2022**, *22*, 7189–7196. [CrossRef]

67. Körük, A.E.; Kankal, M.; Yıldız, M.B.; Akçay, F.; Şan, M.; Nacar, S. Trend analysis of precipitation using innovative approaches in northwestern Turkey. *Phys. Chem. Earth Parts A/B/C* **2023**, *131*, 103416. [CrossRef]

68. Alashan, S. An improved version of innovative trend analyses. *Arab. J. Geosci.* **2018**, *11*, 50. [CrossRef]

69. Ropelewski, C.F.; Halpert, M.S. The Southern Oscillation and Northern Hemisphere Temperature Variability. In *Developments in Atmospheric Science*; Elsevier: Amsterdam, The Netherlands, 1991; Volume 19, pp. 369–376, ISBN 0167-5117.

70. Trenberth, K.E.; Hoar, T.J. El Niño and climate change. *Geophys. Res. Lett.* **1997**, *24*, 3057–3060. [CrossRef]

71. Gupta, V.; Jain, M.K. Impact of ENSO, Global Warming, and Land Surface Elevation on Extreme Precipitation in India. *J. Hydrol. Eng.* **2020**, *25*, 05019032. [CrossRef]

72. Hussain, A.; Cao, J.; Hussain, I.; Begum, S.; Akhtar, M.; Wu, X.; Guan, Y.; Zhou, J. Observed Trends and Variability of Temperature and Precipitation and Their Global Teleconnections in the Upper Indus Basin, Hindukush-Karakoram-Himalaya. *Atmosphere* **2021**, *12*, 973. [CrossRef]

73. Anjum, M.N.; Ding, Y.; Shangguan, D.; Ahmad, I.; Ijaz, M.W.; Farid, H.U.; Yagoub, Y.E.; Zaman, M.; Adnan, M. Performance evaluation of latest integrated multi-satellite retrievals for Global Precipitation Measurement (IMERG) over the northern highlands of Pakistan. *Atmos. Res.* **2018**, *205*, 134–146. [CrossRef]
74. Salma, S.; Rehman, S.; Shah, M.A. Rainfall Trends in Different Climate Zones of Pakistan. *Pak. J. Meteorol.* **2012**, *9*, 37–47.
75. Magaña, V.O.; Vázquez, J.L.; Pérez, J.L.; Pérez, J.B. Geofísica Internacional. *Geofis. Int.* **2003**, *42*, 313–330.
76. Yang, X.; Wu, J.; Liu, J.; Ye, X. Changes of Extreme Precipitation and Possible Influence of ENSO Events in a Humid Basin in China. *Atmosphere* **2021**, *12*, 1522. [CrossRef]
77. Peña-Q, A.J.; Bermudez-F, L.N.; Ramírez-C, C.; Riaño-H, N.M. Oceanic Niño Index as a Tool to Determine the Effect of Weather on Coffee Plantation in Colombia. *Am. J. Exp. Agric.* **2015**, *7*, 395–404. [CrossRef]
78. Bhatti, A.S.; Wang, G.; Ullah, W.; Ullah, S.; Hagan, D.F.T.; Nooni, I.K.; Lou, D.; Ullah, I. Trend in Extreme Precipitation Indices Based on Long Term In Situ Precipitation Records over Pakistan. *Water* **2020**, *12*, 797. [CrossRef]
79. Supari; Tangang, F.; Salimun, E.; Aldrian, E.; Sopaheluwakan, A.; Juneng, L. ENSO modulation of seasonal rainfall and extremes in Indonesia. *Clim. Dyn.* **2017**, *51*, 2559–2580. [CrossRef]
80. Khan, A.H. The Influence of La-Nina Phenomena on Pakistan's Precipitation. *Pak. J. Meteorol.* **2004**, *1*, 23–31.
81. Cai, W.; Borlace, S.; Lengaigne, M.; van Rensch, P.; Collins, M.; Vecchi, G.; Timmermann, A.; Santoso, A.; McPhaden, M.J.; Wu, L.; et al. Increasing frequency of extreme El Niño events due to greenhouse warming. *Nat. Clim. Chang.* **2014**, *4*, 111–116. [CrossRef]